Cellular Microbiology (2015) doi:10.1111/cmi.12415

Infectious bursal disease virus uptake involves macropinocytosis and trafficking to early endosomes in a Rab5-dependent manner

María C. Gimenez,[1,2] José F. Rodríguez Aguirre,[3] María I. Colombo,[1,2]* Laura R. Delgui[1,2,4]**

[1]*Facultad de Farmacia y Bioquímica, Universidad Juan Agustín Maza, Mendoza, Argentina.*
[2]*Instituto de Histología y Embriología (IHEM), Facultad de Ciencias Médicas, Universidad Nacional de Cuyo – CONICET, Mendoza, Argentina.*
[3]*Departamento de Biología Molecular y Celular, Centro Nacional de Biotecnología – CSIC, Madrid, Spain.*
[4]*Facultad de Ciencias Exactas y Naturales, Universidad Nacional de Cuyo, Mendoza, Argentina.*

Summary

Infectious bursal disease virus **(IBDV) internalization is sparsely known in terms of molecular components of the pathway involved. To describe the cell biological features of IBDV endocytosis, we employed perturbants of endocytic pathways such as pharmacological inhibitors and overexpression of dominant-negative mutants. Internalization analysis was performed quantifying infected cells by immunofluorescence and Western blot detection of the viral protein VP3 at 12 h post-infection reinforced by the analysis of the capsid protein VP2 localization after virus uptake at 1 h post-infection. We compared IBDV infection to the internalization of well-established ligands with defined endocytic pathways: transferrin, cholera-toxin subunit B and dextran. To describe virus endocytosis at the morphological level, we performed ultrastructural studies of viral internalization kinetics in control and actin dynamics-blocked cells. Our results indicate that IBDV endocytic internalization was clathrin- and dynamin-independent, and that IBDV uses macropinocytosis as the primary entry mechanism. After uptake, virus traffics to early endosomes and requires exposure to the low endocytic pH as well as a functional endocytic pathway to complete its replication cycle. Moreover, our results indicate that the GTPase Rab5 is crucial for IBDV entry supporting the participation of the early endosomal pathway in IBDV internalization and infection of susceptible cells.**

Received 18 August, 2014; revised 18 December, 2014; accepted 2 January, 2015. For correspondence. *E-mail mcolombo@fcm.uncu.edu.ar; Tel. (+54) 261 5244050; Fax (+54) 261 4494117 int. 7050. **E-mail ldelgui@fcm.uncu.edu.ar; Tel. (+54) 261 5244050; Fax (+54) 261 4494117 int. 7050.

Introduction

Virus replication entails a complex set of interactions between the host cell machinery and viral components, which jointly drive the process of making a new viral progeny. Being obligatory intracellular parasites, viruses have evolved a plethora of strategies allowing them to complete their genetic programme inside the cell. These strategies profit from the vast number of different processes that the eukaryotic cell accomplishes in its life span. Virus uptake is a complex process, which comprises an initial step conducted to deliver their genome into the cytosol (RNA viruses) or the nucleus (DNA viruses). Entry is a multistep process achieved after viral attachment, signalling, endocytosis, penetration and uncoating of the viral genome as has recently been summarized by Yamauchi and Helenius (2013).

Eukaryotic cells carry out different types of endocytosis ranging from receptor-mediated internalization of soluble ligands by clathrin-coated vesicles to the ingestion of large particles by phagocytosis (Conner and Schmid, 2003). These processes differ not only in the nature of the cargo, but also in the cellular factors involved, the signals needed for activation, and the destiny of the internalized material. Among them, macropinocytosis is a transiently triggered, growth factor-induced, actin-dependent endocytic process that results in the internalization of fluid and membrane into large vesicles. A considerable cell-wide plasma membrane ruffling, such as those formed by filopodia and lamellipodia, induced by the activation of actin and microfilaments underneath the plasma membrane is associated to this process (Kerr and Teasdale, 2009). As mentioned, macropinocytosis involves the formation of large vacuoles, and it is primarily used for

non-specific uptake of fluid, solutes, membrane, ligands and smaller particles attached to the plasma membrane. Recent studies have reported that viruses use macropinocytosis as a direct endocytic route for productive infection, reviewed in Mercer and Helenius (2009). A number of relevant human pathogens, including enveloped and non-enveloped viruses, RNA and DNA viruses, as well as large and small viruses, employ macropinocytosis for internalization. Adenovirus (Meier *et al*., 2002; Amstutz *et al*., 2008; Kalin *et al*., 2010), HIV (Marechal *et al*., 2001), influenza A virus (de Vries *et al*., 2011), Ebola virus (Nanbo *et al*., 2010; Saeed *et al*., 2010), Kaposi's sarcoma-associated virus (Valiya Veettil *et al*., 2010), papillomavirus type 16 (Schelhaas *et al*., 2012) and respiratory syncytial virus (Krzyzaniak *et al*., 2013), are examples of viruses that employ macropinocytosis for entry into host cells. Although literature describing this internalization strategy is still scarce, macropinocytic involvement in virus uptake represents a whole field of study as the macropinocytic process itself has not been yet fully characterized. It is important to mention that macrophages and dendritic cells are equipped with macropinocytosis as an ongoing constitutive process, which coupled to the migratory phenotype of these cells is essential for their immune function (Mercer and Greber, 2013).

The *infectious bursal disease virus* (IBDV) is the best characterized member of the *Birnaviridae* family that groups naked icosahedral viruses with bi-segmented double-stranded RNA (dsRNA) genomes (Delmas *et al*., 2005). IBDV infects different avian species and causes an acute immunosuppressive disease, known as infectious bursal disease or Gumboro disease, which affects domestic chickens (*Gallus gallus*) and is responsible for major economic losses to the poultry industry worldwide (van den Berg *et al*., 2000). For around 30 years, classical IBDV strains predominated throughout the world and were effectively controlled by vaccination. The sudden appearance of antigenic variants in the United States, and very virulent strains in Europe in the late 1980s accelerated the introduction of new vaccines based upon variants and less attenuated 'hot' strains, respectively, which lead to it quickly spreading to other regions of the world causing mortalities as high as 80%. Chickens are highly susceptible to the infection between 3 and 6 weeks after hatching. After the ingestion of virus-contaminated stuff, virus particles are taken up by resident gut macrophages, and then transported to other tissues. After reaching the Fabricius bursa, the main IBDV-target organ, the virus actively replicates in B lymphocytes (Monis *et al*., 2006). The loss of lymphocyte populations associated to the infection causes immune suppression and hampers the immunological maturation of infected birds (Sharma *et al*., 2000). IBDV particles possess a single capsid uniquely formed by 260 trimers of the capsid polypeptide VP2 (Bottcher *et al*., 1997). The inner capsid space is occupied by a ribonucleoprotein complex formed by the dsRNA genome wrapped up by the VP3 polypeptide and covalently linked to the bound form of the VP1 RNA-dependent RNA polymerase, and by 'free' VP1 molecules thought to act both as primer and polymerase during RNA transcription (Luque *et al*., 2009).

Recent studies have begun to reveal critical aspects of the initial steps in IBDV replication cycle, cell attachment and internalization. Lin *et al*. (2007) and Delgui *et al*. (2009) described the chicken heat shock protein 90 and the $\alpha4\beta1$ integrin as components of the cellular receptor complex respectively. Moreover, the VP2 $\alpha4\beta1$ integrin-binding motif was identified and shown to be essential for virus attachment and replication (Delgui *et al*., 2009). On the other hand, birnaviruses possess several capsid-embedded peptides thought to play an important role during virus entry. These peptides are by-products generated during the C-terminal proteolytic trimming of the capsid protein precursor. It has been shown that one of them, known as pep 46, contains a membrane-active domain that deforms biological membranes leading to the formation of pores (Galloux *et al*., 2007). It has been hypothesized that after being endocytosed, exchange of small molecules between damaged endosomes and the cytoplasm would allow the initial transcription of the genome. More recently, Leung and collaborators (Yip *et al*., 2012) demonstrated that uncoating of culture-adapted IBDV (caIBDV) required removal of endosomal Ca^{2+} regulated by the vesicular H^{+}-ATPase. By employing pharmacological inhibitors, the authors suggested a particular endocytic pathway involved in virus internalization. However, to our knowledge, a detailed study of the endocytic mechanism involved in IBDV uptake was still missing.

In this study, we addressed IBDV endocytosis by interrupting the function of molecular components associated to the different endocytic mechanisms by two complementary approaches, i.e. the use of pharmacological inhibitors and overexpression of dominant-negative (DN) proteins. Immunofluorescence and Western blot analysis were used to quantify infectivity levels following treatment with specific inhibitors. Moreover, internalization was confirmed by observing virions localization at 1 h post-infection. In addition, thin section electron microscopy of cryo-substituted samples was carried out to analyse the kinetics and morphology of virus internalization. Several well-established endocytic ligands specific for each particular pathway were employed as controls, i.e. transferrin (Trf), cholera-toxin subunit B (CtB) and dextran (Dx). Our results indicate that IBDV endocytosis was clathrin- and dynamin-independent. Here we show that IBDV exploits a macropinocytic pathway dependent

on actin polymerization and on a functional Na^+/H^+ exchanger-1 (NHE-1). Moreover, IBDV particles traffic to endosomal structures in a Rab5-dependent manner, and profit of early endosomal acidification to efficiently infect susceptible host cells.

Results

IBDV internalization is independent of dynamin, clathrin and caveolin

Previous reports suggested that IBDV relays on endocytosis to gain access to susceptible cells (Galloux *et al*., 2007; Yip *et al*., 2012). However, a detailed study elucidating the specific nature of the main endocytic pathway used by the virus was still lacking. In the present report we studied, at the molecular level, IBDV endocytosis following viral attachment to the cell surface. The present study was performed using two well-characterized IBDV-susceptible cell types i.e. QM7, an avian cell line close to the natural IBDV host cellular system; and HeLa, a human cell line that allows the use of molecular tools as yet unavailable for avian cell studies. Unless stated, infections were performed at a multiplicity of infection (MOI) of 1 plaque-forming units per cell (pfu $cell^{-1}$). Virus endocytosis was determined by quantifying the levels of the viral protein VP3 by Western blot and/or by determining the percentage of infected cells by immunofluorescence.

Clathrin-mediated endocytosis (CME) is a major endocytic pathway from the plasma membrane to early endosomes. In CME, in response to receptor-mediated internalization signals, clathrin is assembled on the inner face of the plasma membrane to form a characteristic coated pit. After assembly, coated pits pinch off from the cell surface generating clathrin-coated vesicles (Keen, 1990). Dynamin is a Guanosine-5'-triphosphate (GTPase) that allows the detachment and release of newly formed endocytic vesicles from the plasma membrane (Morlot and Roux, 2013). Several isoforms of dynamin have been described, i.e. dynamin-1 [selectively expressed in neurons (Ferguson *et al*., 2007)]; dynamin-2 [ubiquitously expressed (Cook *et al*., 1994)]; and Drp1, the mitochondrial dynamin. Dymanin-2 contributes to multiple forms of endocytosis, but its action is better understood in the context of CME and its inhibition prevents clathrin-coated vesicle fission from the membrane (Morlot and Roux, 2013). As a first approach, the dynamin role in virus internalization was assessed by employing Dynasore (Dyn), a cell-permeable small molecule that non-competitively inhibits the GTPase activity of dynamin (Macia *et al*., 2006). Additionally, chlorpromazine (CPZ), a cationic amphiphilic molecule that disrupts the assembly of clathrin lattices at the cell surface and on endosomes was also tested (Wang *et al*., 1993). To avoid cytotoxicity, the working dose of both inhibitors was experimentally determined for each cell type. Our results indicate that whereas internalization of the well-characterized CME cargo protein Trf was efficiently prevented by both inhibitors [Figs 1A and S1C (HeLa cells) and Fig. S1A (QM7 cells)], IBDV infection was not hampered by any of these drugs (Fig. 1B and C).

To corroborate that IBDV internalization was indeed dynamin-independent, cells transiently overexpressing enhanced green fluorescent protein (EGFP)-Dyn2K44A, a DN mutant form of dynamin-2 fused to EGFP, were employed (Hernaez and Alonso, 2010). Similar to the effect observed in Dyn-treated cells, EGFP-Dyn2K44A expression caused a significant drop in the internalization of Trf compared with that observed in cells overexpressing EGFP-Dyn2wt (Fig. 1D). However, in contrast to Trf uptake, IBDV infection was not inhibited in HeLa or QM7 cells overexpressing the DN mutant EGFP-Dyn2K44A (Fig. 1E). These findings indicate that IBDV endocytosis is independent of dynamin-2 functionality and clathrin assembly.

Caveolae are flask-shaped invaginations at the plasma membrane that contain caveolin proteins and are the most prominent structures in the specialized membrane microdomains known as lipid rafts (Parton and Richards, 2003). Dynamin has also been implicated in caveolin-dependent internalization and both dynamin and actin were transiently detected at caveolae, coincident with their fission from the plasma membrane (Pelkmans *et al*., 2002). However, the dynamics and function of dynamin at caveolae remains largely undefined. Therefore, to specifically test whether IBDV may employ a caveolin/lipid rafts-mediated pathway, we used two different drugs that interfere with cholesterol disrupting lipid rafts. Filipin III (Fil III) forms multimeric globular complexes with cholesterol at the plasma membrane causing profound distortions on the structure and functions of cholesterol-rich membrane domains, including inhibition of lipid raft ligands internalization (Orlandi and Fishman, 1998), whereas methyl-β-cyclodextrin (MβCD) extracts cholesterol from the plasma membrane (Kilsdonk *et al*., 1995). CtB is a well-characterized molecule known to be internalized by a caveola-mediated pathway (Lu *et al*., 2005). As shown in Fig. 2A (HeLa cells) and Fig. 2B (QM7 cells), the MβCD treatment resulted in a noticeable shift from a punctated cytoplasmic distribution to a predominantly plasma membrane location in both cell lines, whereas Fil III caused a significant reduction on the amount of internalized CtB, indicating that toxin internalization was effectively blocked in HeLa cells, but failed to inhibit CtB uptake in QM7 as shown in Fig. 2B. As observed both by Western blot (Fig. 2C and D) and immunofluorescence (Fig. 2E and F) the IBDV infection was basically unmodified after

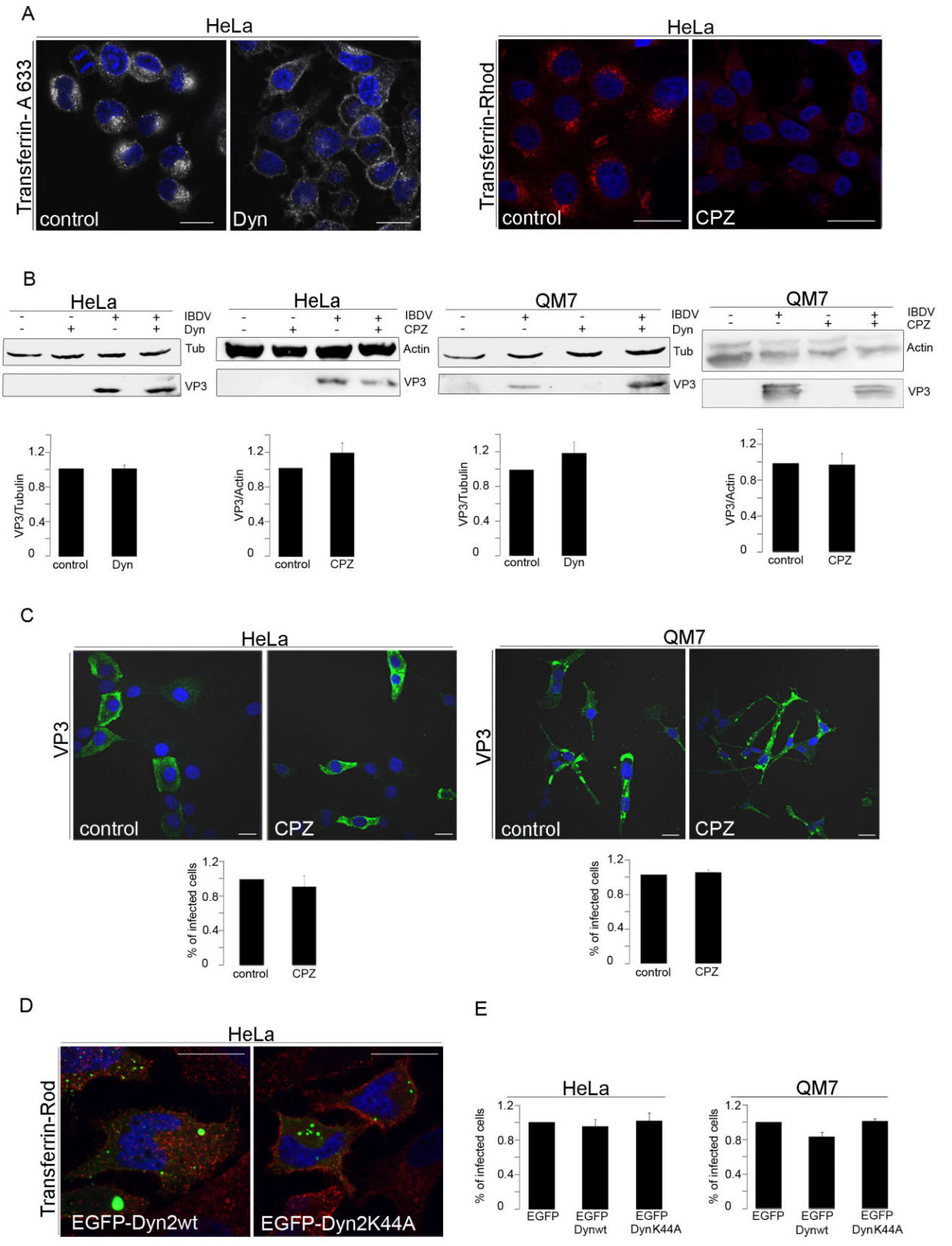

Fig. 1. IBDV entry does not require dynamin activity and is clathrin-independent.
A. HeLa cells untreated or pretreated with 80 μM Dyn or 50 μM CPZ were incubated with Transferrin-Alexa 633 or Transferrin-Rhodamine and extensively washed with PBS to remove the unbound transferrin and processed for immunofluorescence. Mean fluorescence intensity of the fluorophore in each condition was calculated using ImageJ program employing 50 cells (Fig. S1E).
B. HeLa or QM7 cells were pretreated with Dyn or CPZ. After 12 h p.i. cell lysates were prepared for Western blot analysis. Anti-VP3 antibodies were used to determine the levels of intracellular viral protein and mouse anti-tubulin or anti-actin antibodies to determine protein loading. A representative experiment from three independent ones is shown.
C. HeLa or QM7 cells untreated or pretreated with CPZ, were infected and processed for indirect immunofluorescence using anti-VP3 primary antibodies and the corresponding Alexa 488-conjugated secondary antibodies. A representative experiment from three independent ones is shown. In each one, 250 cells per condition were employed for quantification analysis.
D. EGFP-Dyn-2wt or EGFP-Dyn2K44A overexpressing cells were treated as described in (A).
E. QM7 or HeLa cells were transfected as indicated in (D), infected and processed for indirect immunofluorescence using anti-VP3 and the corresponding Cy3-conjugated secondary antibodies. The percentage of infected-transfected cells was determined. Three independent experiments were performed, and 100 infected-transfected cells per condition were employed for quantification analysis. Scale bar represents 20 μm.

treatment of HeLa cells with MβCD or Fil III. Curiously, we observed a significant reduction in infection levels after MβCD treatment in QM7 cells (Fig. 2D and F). This observation was expected to some extent as acute cholesterol depletion by MβCD was shown to cause several non-specific effects on cellular cytoskeleton and signalling, including the dispersion of F-actin, inhibition of phosphatidylinositol turnover and activation of Ras family GTPases (Pike and Miller, 1998; Kranenburg *et al*., 2001; Kanzaki and Pessin, 2002). Moreover, this observed reduction in virus uptake also suggests that IBDV partially exploits caveolin/lipid rafts-mediated pathway in the avian cells, as it has been recently reported by Yip *et al*. (2012).

Our results indicate that infectious IBDV endocytic internalization is independent of clathrin and dynamin in both cellular models and suggest that caveolin/lipid rafts is partially involved in IBDV internalization only in the avian model. Taken together, these results suggest that IBDV internalization relays on different endocytic mechanisms likely dependent on the target cell.

IBDV internalization is an actin-dependent process

Recent studies have implicated the actin cytoskeleton in the regulation of different endocytic pathways (Merrifield, 2004; Kaksonen *et al*., 2006). During phagocytosis and macropinocytosis F-actin polymerization is required to produce outward protrusions of the plasma membrane (i.e. ruffles). In addition, actin polymerization has been involved in caveolar/lipid raft endocytosis, and other endocytic pathways including those mediated by IL-2 and Arf6 (Doherty and McMahon, 2009; Mercer *et al*., 2010).

To test the involvement of actin, we used the actin-depolymerizing agents cytochalasin D (Cyto D) and latrunculin B (Lat B) (Peterson and Mitchison, 2002). As expected, these drugs strongly disrupted the actin polymers and efficiently inhibited the uptake of a 70 kDa Dx-Texas red, a soluble fluorescent tracer known to be up taken by an actin-dependent pathway (Ohkuma and Poole, 1978) [Fig. 3A (HeLa cells) and Fig. S1B (QM7 cells)]. In addition, both drugs efficiently inhibited IBDV infection determined by both immunofluorescence (Fig. 3B) and Western blot analysis (Fig. 3C). Therefore, these results indicate that functional actin dynamics are required for IBDV infection.

Macropinocytosis is a mechanism of endocytosis, which involves trapping large fluid droplets by ruffle extensions formed at the cell surface (Doherty and McMahon, 2009). It is known that actin polymerization is critical for the formation of these macropinocytic protrusions of the plasma membrane. In addition, it has been shown that macropinosome formation requires Na^+/H^+ exchanger (NHE) activity (Koivusalo *et al*., 2010). NHE is an integral plasma membrane protein and is typically involved in the exchange of intracellular H^+ with external Na^+, according to the concentration gradient (Kojima *et al*., 2012). NHE belongs to a family consisting of 10 members (NHE-1–10) that are present in almost all living cells, NHE-1 being the most ubiquitously expressed (Karmazyn, 2013). As the participation of NHE has become one the diagnostic criteria for macropinocytosis, we decided to study the role of NHE in IBDV infection (Mercer and Helenius, 2009). We first determined the expression and cellular distribution of NHE-1 in our cell lines employing specific antibodies. A well-defined plasma membrane distribution was observed in both cell types (data not shown). It has been shown that inhibition of NHE-1 blocks macropinocytosis. Amiloride, a guanidinium-containing pyrazine derivative, has been extensively used as an inhibitor of NHEs (Orlowski and Grinstein, 2004). However, amiloride is neither a universal nor a specific inhibitor of NHE. Thus, to increase the potency and selectivity of NHE inhibitors several amiloride analogues have been synthesized, including ethylisopropylamiloride [EIPA, (Masereel *et al*., 2003)]. EIPA inhibits NHE-1 functionality and when Na^+/H^+ exchange is impaired, the H^+ generated during actin polymerization signalling (activation of Rac1 and Cdc42) inhibits macropinocytosis (Koivusalo *et al*., 2010). Therefore, to assess the role of macropinocytosis we used

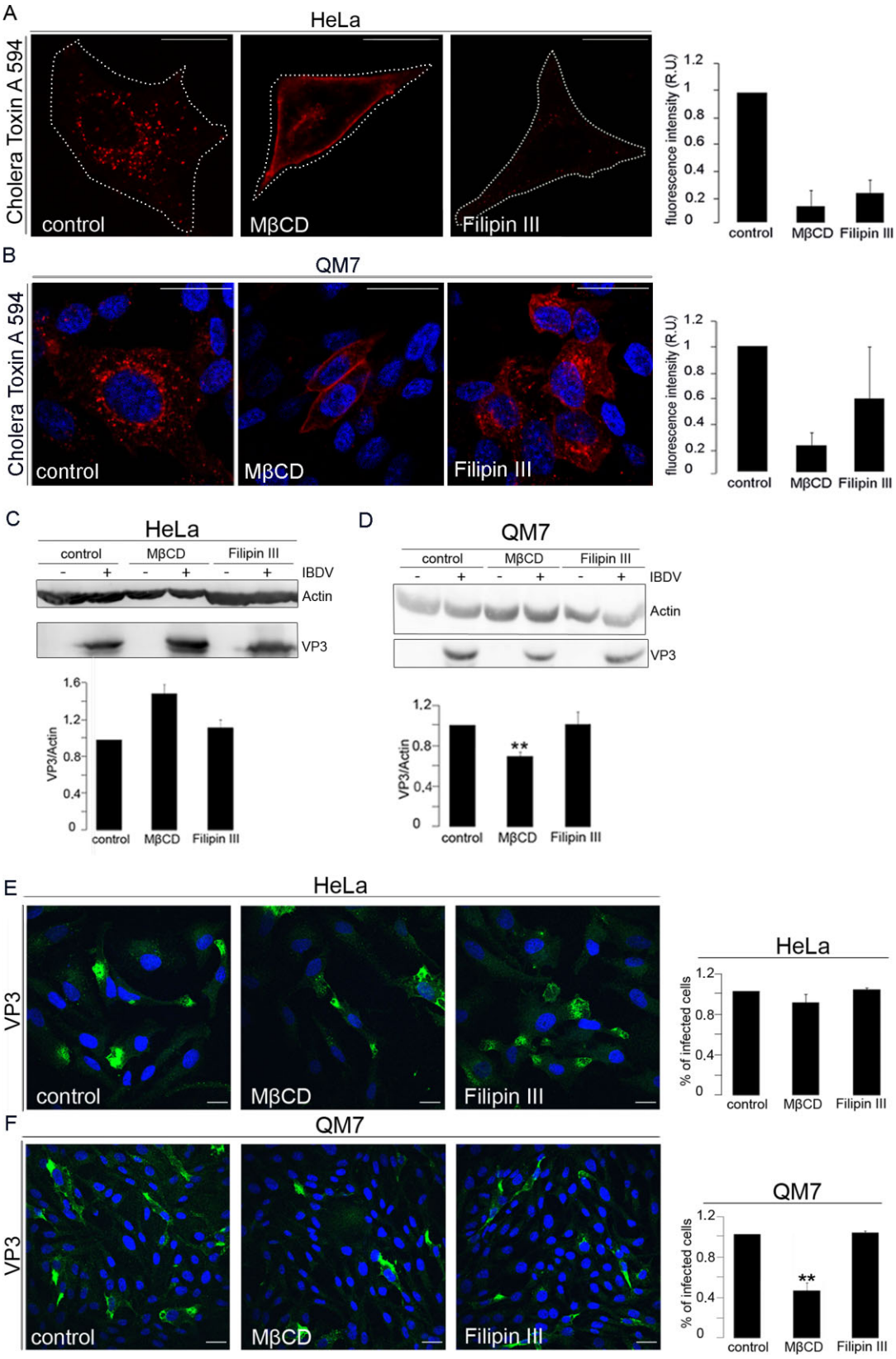

Fig. 2. IBDV infection is caveolin-independent. (A) HeLa or (B) QM7 cells untreated or pretreated with MβCD or Fil III were incubated with Alexa-Fluor 594-CtB and extensively washed with PBS to remove the unbound reagent. Cells were fixed and analysed by CLSM. Representative images are shown. Mean fluorescence intensity of the fluorophore in each condition was calculated using ImageJ program employing 50 cells (C) HeLa or (D) QM7 cells were pretreated with MβCD or Fil III, infected and processed for Western blot analysis. Anti-VP3 antibodies were used to determine the levels of intracellular viral protein and mouse anti-actin antibodies for protein loading. A representative experiment from three independent ones is shown (**$P < 0.1$) (E) HeLa cells or QM7 cells were pretreated with MβCD or Fil III, infected and processed for indirect immunofluorescence using anti-VP3 primary antibodies and the corresponding Alexa 488-conjugated secondary antibodies. Percentage of infected cells in (E) and (F) were determined (**$P < 0.1$). Three independent experiments were performed, and 250 cells per condition in each experiment were scored in the quantification analysis. Scale bar represent 20 μm.

EIPA, which efficiently inhibited the uptake of Dx-Texas red [Fig. 3D (HeLa cells) and Fig. S1B (QM7 cells)]. Likewise, a marked decrease in IBDV infection was observed in EIPA-treated cells analysed both by Western blot (Fig. 3E) and by immunofluorescence (Fig. 3F). These results strongly point that the virus utilizes macropinocytosis to be internalized into host cells.

IBDV induces fluid phase uptake

The reliance of IBDV entry on actin cytoskeleton integrity and its dependence on a functional Na^+/H^+ exchanger (NHE-1) suggest that infectious internalization of IBDV occurred via macropinocytosis, as recently shown for several other viruses [for reviews see Mercer and Helenius (2009; 2012)]. One of the characteristic features of macropinocytosis is an elevation in the uptake of extracellular fluid (Norbury, 2006). Indeed, when serum-starved QM7 cells were exposed to 10% foetal calf serum (FCS) or IBDV particles, we observed that internalization of 70 kDa Dx-Texas red, a soluble fluorescent tracer added to the medium, showed a significant increase of 116% and 123% over control cells respectively. Moreover, this IBDV-induced increase in Dx-Texas red uptake was severely inhibited in EIPA-treated cells, evidenced by a decrease in Dx uptake, which was 31% compared with control cells (Fig. 4A). Concomitantly, colocalization analysis performed at 1 h p.i. showed that (50 ± 3)% of endocytosed viruses stained by anti-VP2 antibodies were localized in Dx-Texas red filled, intracellular vesicles (Fig. 4B, upper panels). In contrast, in EIPA-treated cells, the labelling of both markers remained at the cell membrane, as expected (Fig. 4B, lower panels). Thus, these results comprise a clear demonstration that IBDV induces macropinocytosis and exploits this pathway for virus endocytosis and infection.

Macropinocytosis-mediated uptake of IBDV

The data obtained point to macropinocytosis as the main endocytic pathway for IBDV. For further analysis, using thin-section transmission electron microscopy, we analysed the morphology of IBDV internalization process in HeLa cells. At 15 min p.i. most detected virions were attached to the external surface of the plasma membrane, occasionally forming slight membrane indentations. A relatively common finding was the presence of small clusters of two or more virus particles attached to the cell membrane (Fig. 5A, 15 min). At 45 min p.i., virions were prevalently found in close proximity to or at the base of cellular protrusions resembling membrane ruffles (Fig. 5A, 45 min). At 60 min p.i., virions were mainly trapped in membrane indentations, occasionally holding several virus particles, or in vesicles lacking a perceptible coat accommodating multiple virions. (Fig. 5A, 60 min). The size (> 300 nm in diameter) of the detected virus-containing vesicles is larger than that expected for other endocytic pathways (Mercer and Helenius, 2009), thus reinforcing the notion that macropinocytosis is the main pathway employed by IBD virus to gain access to susceptible cells.

When virus internalization was blocked by inhibiting actin polymerization with Cyto D or Lat B, at 60 min p.i., particles were mainly found in tight rows located in narrow tubular invaginations of the plasma membrane (Fig. 5B). Moreover, after Lat B treatment, most viruses were localized in plasma membrane invaginations, suggesting that they had sunk into the plasma membrane instead of having been actively engulfed (Fig. 5B). This observation suggests a role of actin polymerization in scission of virus-containing macropinosomes. Indeed, Liebl and Griffiths (2009) recently reported that the actin coat has a role in compression-induced budding of macropinosomes, followed either by propulsion or by complete scission of the organelle. Similar structural observations were also described for the *human papillomavirus* type 16 (Schelhaas *et al*., 2012). As a control of virus size and morphology, we employed thin sections of HeLa cells infected with IBDV for 36 h containing typical para-crystaline IBDV arrays (Fig. 5B, control).

To further analyse the role of actin, we examined by confocal microscopy whether viral infection causes rearrangements of the actin cytoskeleton in HeLa cells by using phalloidin-staining. We observed a dramatic change in actin distribution after virus uptake. The number of actin stress fibres decreased, the cells rounded up, and transient blebs filled with actin formed at the cell surface (Fig. 5C). These changes were quantitated determining the number of cells with 'disorganized actin filaments' in mock – versus IBDV-infected cells showing a clear shift of

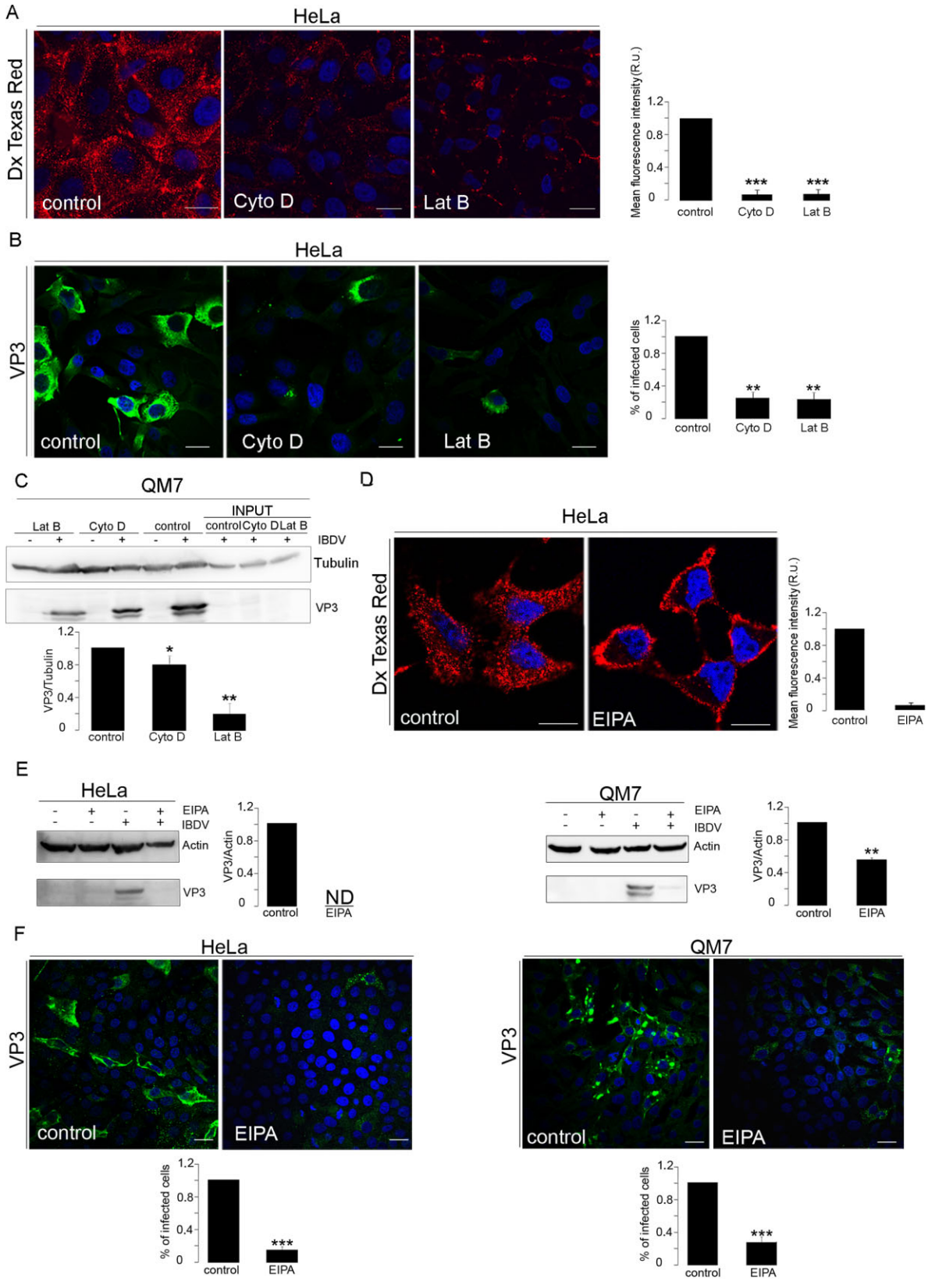

Fig. 3. Role of actin and macropinocytosis in IBDV infection.
A. HeLa cells were untreated or pretreated with Cyto D or with Lat B, incubated with Dextran-Texas Red and analysed by confocal microscopy. Representative images are shown. Mean fluorescence intensity of the fluorophore in each condition was calculated employing 50 cells (**$P < 0.1$, ***$P < 0.01$).
B. HeLa cells were untreated or pretreated with Cyto D or with Lat B, infected and processed for indirect immunofluorescence using anti-VP3 primary antibodies and the corresponding Alexa 488-conjugated secondary antibodies. A representative experiment from three independent ones is shown. In each one, 250 infected cells per condition were scored for quantification analysis (**$P < 0.1$).
C. QM7 cells pretreated with Cyto D or Lat B were infected and 12 h p.i. (or 0 h p.i. for INPUT controls) were processed for Western blot analysis. Anti-VP3 antibodies were used to determine levels of intracellular viral protein and mouse anti-tubulin for protein loading. A representative experiment from three independent ones is shown (*$P < 0.5$, **$P < 0.1$).
D. HeLa cells untreated or pretreated with EIPA were incubated with Dx-Texas Red and extensively washed with PBS-citric acid (pH 5.5) to remove the unbound dextran. Cells were fixed and analysed. Mean fluorescence intensity of the fluorophore in each condition was calculated using ImageJ program employing 50 cells.
E. HeLa or QM7 cells were pretreated with EIPA, infected and processed for Western blot analysis. Anti-VP3 antibodies were used to determine the levels of intracellular viral protein and mouse anti-actin antibodies to determine protein loading. A representative experiment from three independent ones is shown (**$P < 0.1$).
F. HeLa or QM7 cells were untreated or pretreated with EIPA, infected and processed for indirect immunofluorescence using anti-VP3 and the corresponding Alexa 488-conjugated secondary antibodies. A representative experiment from three independent ones is shown (***$P < 0.01$). In each one 250 infected cells per condition were scored. Scale bars represent 20 μm.

actin distribution from normal to disorganized actin after virus contact with the cells (Fig. 5C).

Taken together, all these data strongly point to macropinocytosis as the pathway mainly involved in IBDV internalization and further reinforce the requirement of actin polymerization for efficient virus uptake.

IBDV internalization depends on macropinocytic cellular regulators

Macropinocytosis depends on several kinases (Liberali *et al*., 2008) such as phosphatidylinositol 3-kinase (PI3K). It has been described that PI3K and its effectors induce the formation of lipid structures in ruffles and macropinocytic cups involved in cytoskeleton modulation (Lindmo and Stenmark, 2006; Araki *et al*., 2007). Therefore, we explored PI3K involvement in IBDV internalization by inhibiting its activity with wortmannin (Wort). We observed a significant decrease in virus internalization (Fig. 6A and B), further supporting the role of macropinocytosis in IBDV internalization in both cells models.

Rho GTPases constitute one of the five distinct families of the Ras superfamily (Rojas *et al*., 2012) and are known to be master regulators of the actin cytoskeleton. Although 20 different Rho GTPases have been identified in mammals, attention has focused predominantly on the three most common members of the family: RhoA, Rac1 and Cdc42. Like Ras, the majority of the Rho family members act as molecular switches to regulate signal transduction pathways, by interconverting between inactive Guanosine diphosphate (GDP)-bound and active GTP-bound conformational states (Ridley, 2006). Typically, Rho is involved in the formation of focal adhesion and stress fibres and it has been involved in phagocytosis and caveolar/lipid raft endocytosis (Niedergang and Chavrier, 2005; Mercer *et al*., 2010), whereas Rac forms lamellipodia and/or membrane ruffles, and Cdc42 forms filopodia (Nobes and Hall, 1995; Hall, 1998; Hall and Nobes, 2000). In the process of macropinocytosis, Rac1 is crucial for membrane ruffling and macropinosome formation in a variety of different cell types, including dendrite cells, macrophages, fibroblasts and epithelial cells. Cdc42 activation has also been shown in some cell types during macropinocytosis, although its requirement for macropinocytosis has not been established (Patel and Galan, 2006). To further assess the actin involvement in IBDV internalization, we infected cells overexpressing the dominant-negative mutant forms of RhoA, Rac1 and Cdc42. As expected we observed a marked inhibition of virus internalization in QM7 cells overexpressing RhoA- or Rac1 mutants whereas no effect was observed in cells overexpressing the Cdc42 DN mutant (Fig. 6C). Furthermore, we explored the role of the RhoA effector ROCK employing a specific inhibitor, Y-27632 dihydrochloride (Y-27632). As shown in Fig. 6D, we observed a slight, but statistically significant impairment in IBDV internalization compared with the control situation after ROCK inhibition, reinforcing the RhoA role in virus uptake.

Taken together, these results further reinforce macropinocytosis involvement as the major internalization pathway employed by IBDV and that the actin cytoskeleton has a critical role in the process.

Intracellular trafficking and the role of Rabs in IBDV internalization

After detaching from the plasma membrane, macropinosomes move deeper into the cytoplasm trafficking through a poorly characterized pathway. However, it has been shown that they acidify, and like typical endosomes, acquire Rab5 followed by Rab7 recruitment before becoming endolysosomes (West *et al*., 1989; Rupper

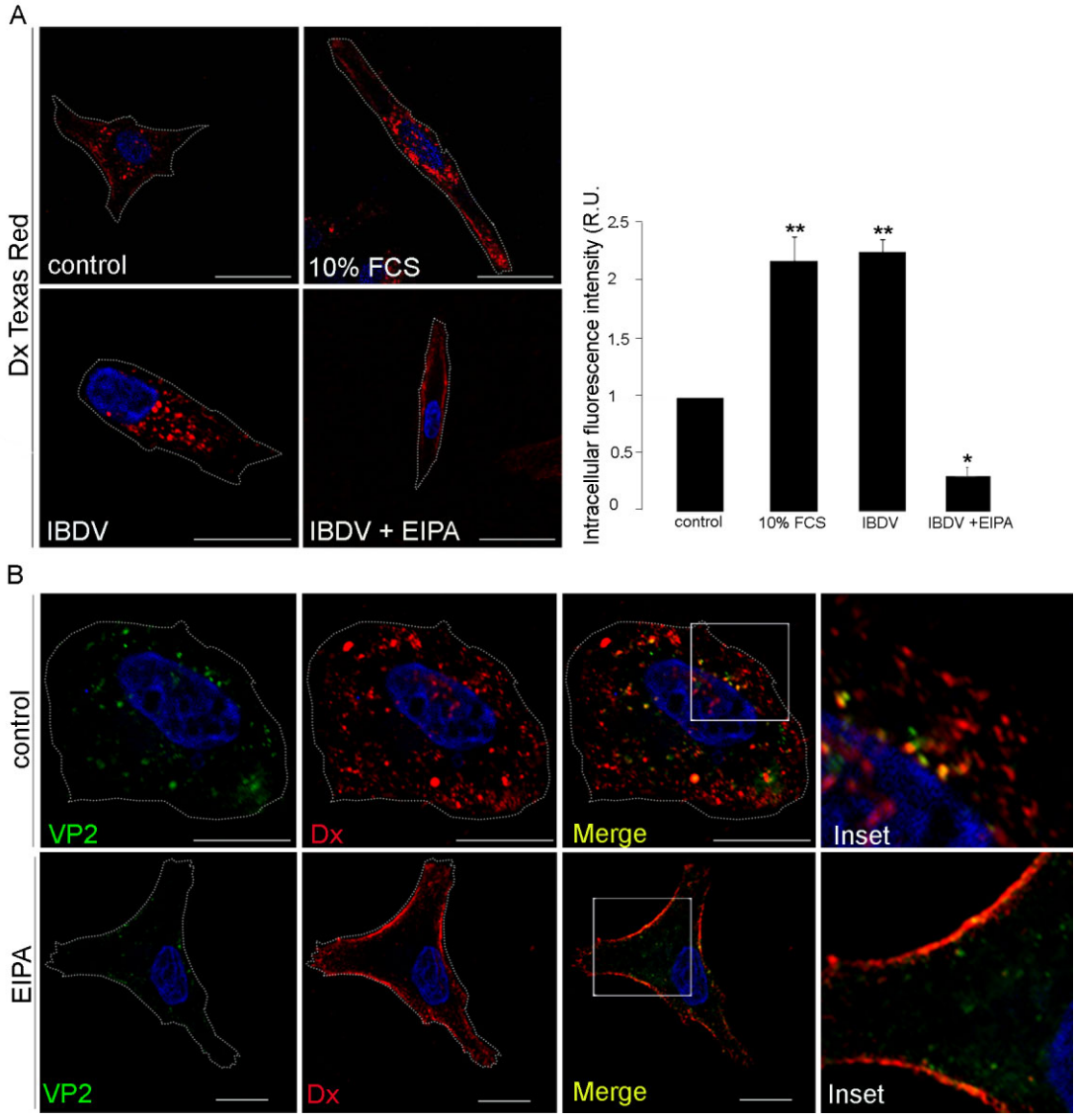

Fig. 4. IBDV stimulates macropinocytosis.
A. Serum-starved QM7 cells were incubated with DMEM medium, FCS supplemented DMEM medium, IBDV or EIPA followed by IBDV. At the same time, 70 kDa Dx Texas red was added in each condition. Afterwards, cells were extensively washed with PBS-citric acid (pH 5.5) to remove the unbound Dextran, and processed for CLSM. Intracellular fluorescence intensity was measured using the ImageJ program. A representative experiment from three independent ones is shown (*$P < 0.5$; **$P < 0.1$). In each one, 30 cells per condition were scored. Scale bars represent 20 μm.
B. QM7 cells were untreated or pretreated with EIPA, and infected. At the same time, Dx-Texas 70 kD red was added in each conditions. Afterwards, cells were extensively washed with PBS-citric acid (pH 5.5) to remove the unbound Dextran and then processed for indirect immunofluorescence using anti-VP2 and the corresponding Alexa 488-conjugated secondary antibodies. The insets show colocalization of VP2 with Dextran, inside the cytoplasm (control condition) or attached to the plasma membrane (EIPA condition). Images of a representative experiment from three independent ones are shown. Scale bars represent 10 μm.

et al., 2001; Schelhaas *et al.*, 2012). Therefore, we next assessed whether IBDV infection occurs in a pH-dependent manner. For this purpose, we employed the weak base NH_4Cl, which neutralizes intravesicular pH, and Bafilomycin A1 (Baf A), which specifically inhibits the H^+-ATPase responsible for intravesicular acidification (Marshansky and Futai, 2008). We found that both compounds markedly altered LysoTracker (Lys) staining of treated cells (Fig. S2A) and significantly impair the ability of IBDV to infect HeLa cells as determined by immunofluorescence (Fig. 7A) and QM7 cells analysed by Western blot (Fig. 7B).

The family of small Rab GTPases plays a crucial role in membrane trafficking of eukaryotic cells, regulating tethering, docking and fusion events among different compartments (Zerial and McBride, 2001). Rab5 regulates the

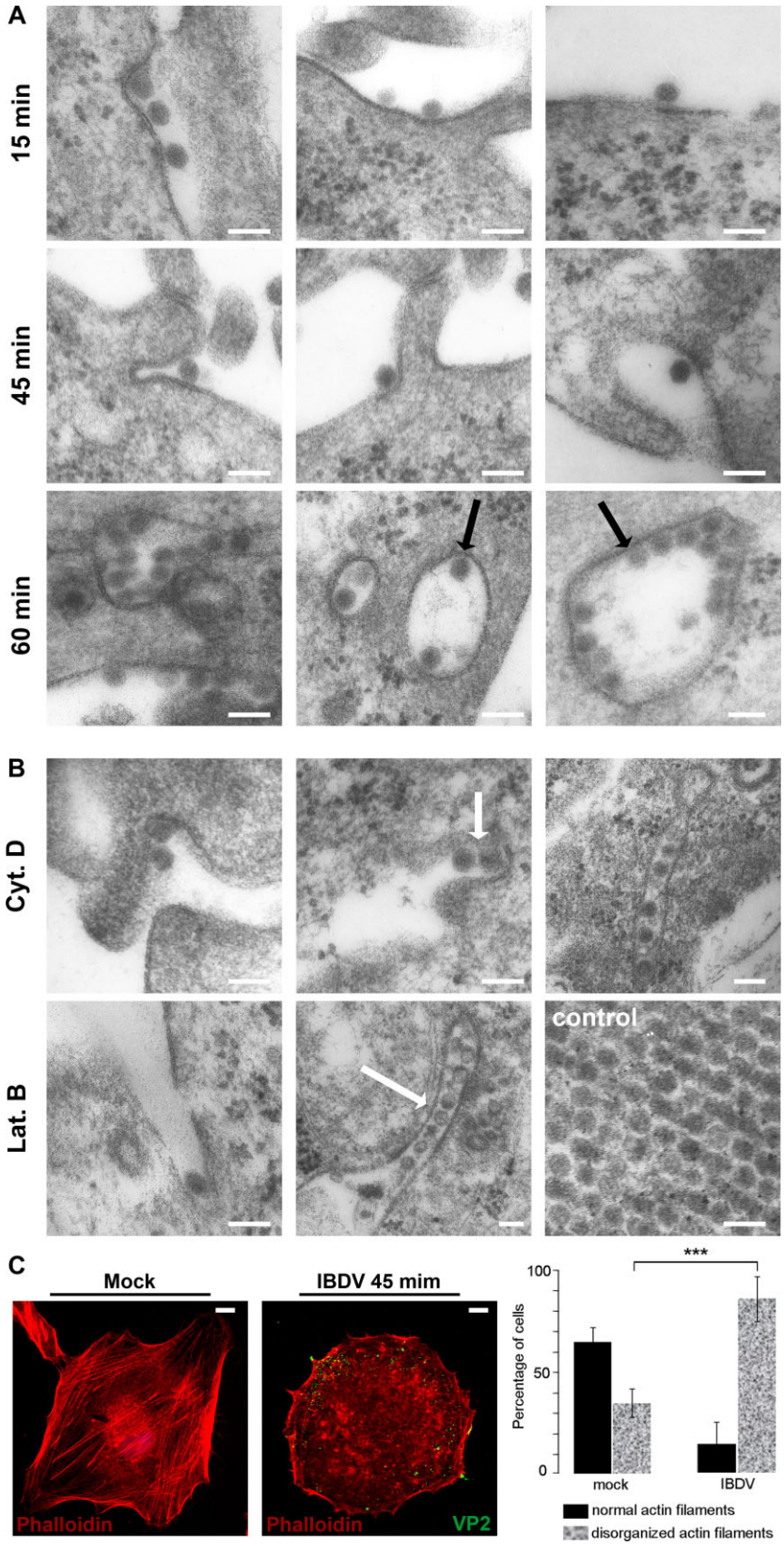

Fig. 5. Actin rearrangements during virus internalization. Infected HeLa cells were either untreated (A) or treated with Cyto D or Lat B (B) throughout infection. Cells were processed for thin section transmission electron microscopy. Representative micrographs of untreated cells (A) at 15 min p.i., 45 min p.i. and 60 min p.i. and treated cells (B) are depicted. For the purpose of corroborating the virus morphology, a micrograph showing a detail of an IBDV paracrystaline array is shown (B, control). Black arrows indicate virus-containing vesicles of 300 and 600 nm sizes approximately. White arrows indicate the smallest and the largest tubular structures ranging from 167 to 890 nm respectively. Scale bars represent 100 nm (C) HeLa cells were incubated in control conditions (mock) or infected with IBDV for 45 min prior to fixation and then processed for indirect immunofluorescence using anti-VP2 and the corresponding Alexa 488-conjugated secondary antibodies. Actin was labelled by incubating the cells with Phalloidin-Rhodamine (1:200) for 1 h at 37°C. Nuclei were stained with Hoechst (blue) and the coverslips were analysed by CLSM. Representative images from three independent experiments are shown (***$P < 0.01$). In each one, 30 cells per condition were scored. Scale bars represent 10 μm.

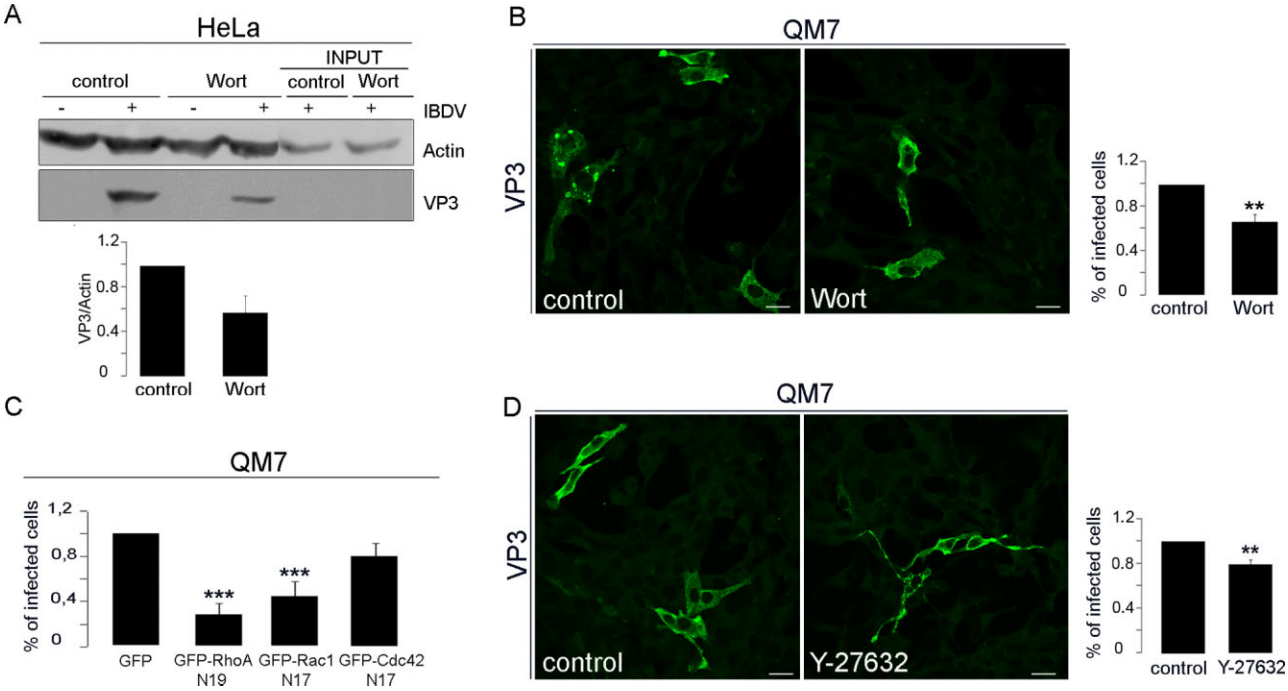

Fig. 6. IBDV internalization depends on macropinocytosis cellular regulators.
A. HeLa cells untreated or pretreated with 100 nM Wort were infected and at 12 h p.i. (or 0 h p.i. for INPUT control) cell lysates were prepared for Western blot analysis. Anti-VP3 antibodies were used to determine the levels of intracellular viral protein and mouse anti-actin antibodies for protein loading. A representative experiment from three independent ones is shown.
B. QM7 cells were untreated or pretreated with 100 nM Wort and infected and processed for indirect immunofluorescence using anti-VP3 and the corresponding Alexa 488-conjugated secondary antibodies. Images of a representative experiment from three independent ones are depicted (**$P < 0.01$). For the quantification 150 infected cells per condition were scored. Scale bars represent 20 μm.
C. QM7 cells were transfected with EGFP or EGFP-tagged forms of the dominant-negative mutants of the Rho Family of GTPases RhoA N19, Rac1 N17 or Cdc42N17. At 24 h post-transfection cells were infected and processed for indirect immunofluorescence using anti-VP3 primary antibodies and the corresponding Cy3-conjugated secondary antibodies. The percentage of transfected-infected cells was determined. Three independent experiments were performed and 100 infected transfected cells per condition in each one were scored for quantification analysis (***$P < 0.01$).
D. QM7 cells were untreated or pretreated with 10 μM Y-27632, infected and processed for indirect immunofluorescence using anti-VP3 and the corresponding Alexa 488-conjugated secondary antibodies. A representative experiment from three independent ones is shown (**$P < 0.01$). In each one 150 infected cells per condition were scored. Scale bars represent 20 μm.

Fig. 7. IBDV trafficking involves early endosomes.
A. HeLa cells untreated or pretreated with NH_4Cl or Baf A1 were infected and processed for indirect immunofluorescence using anti-VP3 primary antibodies and the corresponding Alexa 488-conjugated secondary antibodies. A representative experiment from three independent ones is shown (*$P < 0.5$). In each experiment, 250 infected cells per condition were scored.
B. QM7 cells were untreated or pretreated with NH_4Cl or BafA1, infected and processed for Western blot analysis. VP3 antibodies were used to determine the levels of intracellular viral protein and anti-tubulin antibodies for protein loading. A representative experiment from three independent ones is shown (*$P < 0.5$; **$P < 0.1$).
C. HeLa or QM7 cells were transfected with EGFP or EGFP-tagged forms of wild type Rab5, DN Rab5 mutant (S34N), wild type Rab7 or DN Rab7 mutant (T22N). At 24 h post-transfection cells were infected and after 24 or 12 h p.i., respectively, cells were washed and processed for indirect immunofluorescence using anti-VP3 primary antibodies and the corresponding Cy3-conjugated secondary antibodies. Percentage of transfected-infected cells was determined in each experiment. Three independent experiments were performed and 100 infected transfected cells per condition in each one were scored for quantification analysis. (*$P < 0.5$; **$P < 0.1$; ***$P < 0.001$).
D. QM7 cells transfected with GFP-tagged forms of wild type Rab5 were infected and processed for indirect immunofluorescence using anti-VP2 primary antibodies and the corresponding Alexa 594-conjugated secondary antibodies. The inset shows the colocalization of VP2 with Rab5-positive vesicles. Images are representative of three independent experiments.
E. QM7 cells transfected with GFP-tagged forms of the constitutive active mutant Rab5 were infected and processed for indirect immunofluorescence using anti-VP2 primary antibodies and the corresponding Alexa 594-conjugated secondary antibodies. The inset shows a representative image depicting virions inside large Rab5-positive vesicles. Images are representative of three independent experiments. Scale bars represent 20 μm.

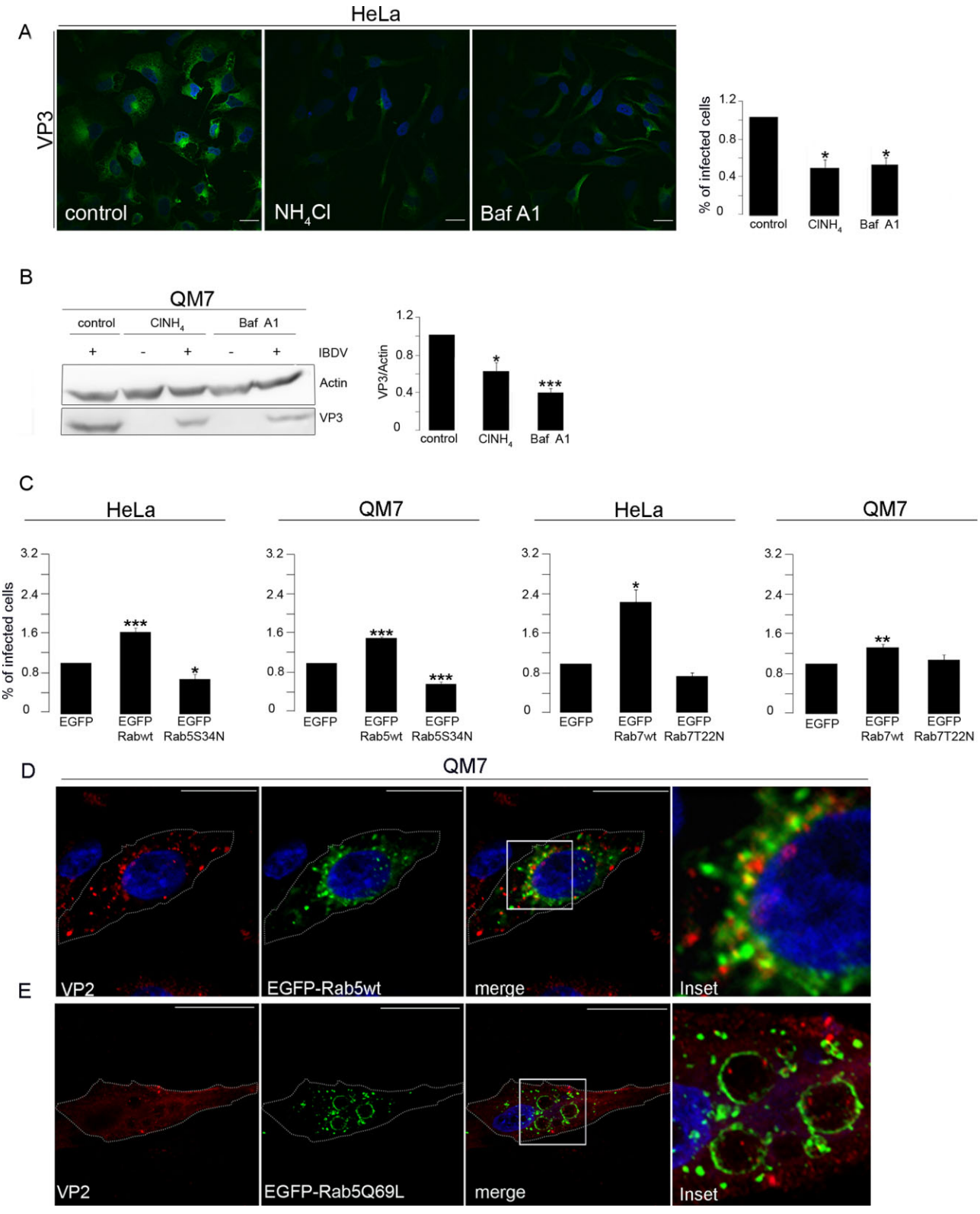

homotypic tethering and fusion of early endosomes (Gorvel *et al*., 1991), while Rab7 is a Rab protein more specifically related with degradative compartments such us late endosomes and lysosomes (Feng *et al*., 1995; Vitelli *et al*., 1997). Therefore, we next assessed the role for endocytic Rab GTPases in IBDV infection. First, we infected HeLa or QM7 cells transiently overexpressing EGFP, the EGFP-Rab5wt or the DN GTP-binding defective EGFP-Rab5S34N and the percentage of transfected-infected cells at 24 h p.i. (in HeLa cells) or 12 h p.i. (in QM7 cells) was determined. It has been shown that overexpression of this Rab5 mutant blocks both receptor-mediated and fluid phase endocytosis and prevents fusion of early endocytic vesicles (Bucci *et al*., 1992; Li and Stahl, 1993). As shown in Fig. S2B, EGFP-Rab5S34N effectively blocked fluid phase endocytosis as determined by the uptake of the tracer Dx-Texas red. Infected cells were visualized by detecting the viral protein VP3 by immunofluorescence. We found a significant increase in infection when EGFP-Rab5wt was overexpressed compared with the EGFP-overexpressing control cells, whereas a moderate but significant decrease was observed in cells overexpressing the DN mutant form of Rab5 (i.e. EGFP-Rab5S34N) (Fig. 7C, left panels).

To test the role of Rab7 in IBDV infection, we employed HeLa or QM7 cells transiently overexpressing EGFP, the EGFP-Rab7wt or the DN mutant EGFP-Rab7T22N and the percentage of transfected-infected cells was determined as described earlier. The DN form of Rab7 prevents transport from early to late endosomes (Feng *et al*., 1995). As depicted in Fig. S2C the inhibitory effect was corroborated by incubating EGFP-Rab7T22N-transfected cells with the self-quenched red Bodipy dye conjugated to BSA (DQ-BSA), which requires enzymatic cleavage in an acidic intracellular compartment to generate a highly fluorescent product. As shown in Fig. 7C (right panels), we found a substantial increase in virus infection when EGFP-Rab7wt was overexpressed whereas the presence of overexpressed DN mutant of EGFP-Rab7 did not significantly affected IBDV infection.

With the purpose of analysing virus trafficking after internalization, we performed colocalization studies at 1 h p.i. employing EGFP-Rab5wt as early endosomal vesicles tracer and antibodies to VP2 to detect incoming virions. Out of three independent experiments, we found $(16 \pm 10)\%$ of colocalization between both structures, which we consider significant taking into account the transient nature of an early endosome. Indeed, this relatively low level of colocalization is similar to earlier reports studying adenovirus (Gastaldelli *et al*., 2008). A representative image is shown in Fig. 7D. Moreover, we assessed the constitutively active mutant EGFP-Rab5Q79L, which when overexpressed induces the formation of enlarged Rab5-positive vesicles that fail to undergo further maturation (Stenmark *et al*., 1994). We took advantage of the particular phenotype obtained with this mutant, which allowed us to more easily detect virion particles inside the enlarged vesicles reinforcing the notion that the virus traffics through Rab5-positive vesicles (Fig. 7E).

All together, our data indicate that early endosome acidification is required for IBDV infection and that internalized virions traffic to Rab5-positive endosomal vesicles where a functional GTPase Rab5 is critical for IBDV replication cycle progress.

Discussion

Internalization of the vast majority of mammalian viruses relies on endocytic mechanisms that transport virus particles from the plasma membrane to the cytoplasm of the host cell. In our report, we present several lines of evidence showing that clathrin and dynamin are dispensable for virus entry, whereas the actin cytoskeleton plays a critical role in virus internalization. Our findings rely on the employment of two evolutionary distant cell lines to perform all the experiments: HeLa (human) and QM7 (avian) cells. Based on the observed conspicuous effect of macropinocytic-specific disruptors in IBDV endocytosis, our results strongly indicate that a macropinocytic pathway is used as the major cellular mechanism for IBDV internalization. Indeed, the reduction of VP3 expression (an indicator of infected cells) by about 80% after EIPA-treatment (a well-described inhibitor of NHE-1 functionality) clearly demonstrated that IBDV uptake by macropinocytosis results in a productive infection. On the other hand, taking into account that actin also plays a role in other endocytic events such as caveolae/lipid rafts endocytosis (Pelkmans *et al*., 2002), and the fact that virus internalization was significantly reduced after cholesterol depletion by MβCD, our results also suggest a caveolin/lipid rafts partial involvement in virus internalization into avian cells, as it has been previously reported by Yip *et al*. (2012). The involvement of RhoA may also support the notion that caveolin/lipid rafts are partially involved in IBDV internalization in the avian model. However, as it has been demonstrated that dynamin has a role in caveolar-mediated endocytosis (Menon and Schafer, 2013), the lack of dynamin involvement in IBDV entry argue against a caveolin participation in virus internalization. Nevertheless, it is important to take into account that data about dynamin involvement in caveolin/lipid rafts in avian cells are still lacking. Thus, to date, cholesterol involvement in IBDV internalization is clearly demonstrated, but data showing its specific contribution is still missing.

After endocytic internalization, most viruses are delivered to endosomes and their subsequent uncoating and cytoplasm invasion occurs from early or late endocytic

structures. Macropinocytic-related mechanisms of virus uptake have a less well-characterized destination. We have shown that in cells overexpressing EGFP-Rab5wt, which have an increased rate of endocytosis (Mukhopadhyay *et al*., 1997), a marked increase in virus internalization was observed. On the other hand, a strong impairment in virus internalization occurred when cells overexpressed the DN form of Rab5, indicating a requirement of an early endocytic pathway regulated by Rab5 for virus entry. However, although overexpression of Rab7wt produced an increase in virus infection because of the augmented rate of the pathway (Mukhopadhyay *et al*., 1997), Rab7 does not seem to be required as overexpression of a DN form of the protein did not impair viral internalization. These findings are in complete agreement with our recent study showing that IBDV replication-complexes are located in endosomal vesicles bearing features of early and intermediate endosomes, but lacking Rab7 and degradative activity (Delgui *et al*., 2013). Also, this is consistent with the idea that virions may escape from the endocytic compartments before fusion with lysosomes to avoid degradation. Moreover, cells overexpressing the constitutive active mutant EGFP-Rab5Q79L, which strongly stimulates not only the rate of endocytosis but also homotypic fusion of early endosomes (Stenmark *et al*., 1994), showed a marked accumulation of viral proteins inside the huge Rab5-positive vesicles generated. The fact that overexpression of EGFP-Rab5Q79L, the GTPase-deficient mutant markedly increases the infection levels is supported by the well-known effect of this mutant in blocking the progression and the maturation of the endocytic pathway (Stenmark *et al*., 1994; Rink *et al*., 2005) (data not shown). These observations reinforce the already stated notion that IBDV replication-complexes localize in endosomal structures avoiding normal endocytosis progression. In summary, the requirement for Rab5 and a functional early endocytic pathway in IBDV internalization is a complete novel finding in the Birnaviruses field and an important point towards linking viral internalization and replication mechanisms.

Macropinocytosis differs from other endocytic pathways in that it involves an extensive actin cytoskeletal reorganization linked to an outward-directed formation of plasma membrane extensions, whereas in other pathways, the plasma membrane buds into the cell. Under normal conditions, macropinocytosis is induced by growth factors, and depending on cell type and the stimulus, formation of membrane ruffles, filopodia or blebs precedes the generation of large vesicles named macropinosomes (Swanson and Watts, 1995). To trigger macropinocytosis, viruses must establish contact with specific surface molecules (i.e. receptor tyrosine kinases, phosphatidylserine-receptor, integrins) capable of activating the appropriate signalling pathways, which lead to actin rearrangements and plasma membrane protrusions. Several viral agents exploiting macropinocytosis to gain entry into the host cells take advantage of integrin-binding, i.e. adenoviruses 3 and 35 to αv-integrins and CD46; echovirus 1 to $\alpha 2\beta 1$ integrins; Kaposi's sarcoma-associated herpes virus to $\alpha 3\beta 1$, $\alpha v\beta 3$, and $\alpha v\beta 5$ integrins (Amstutz *et al*., 2008; Karjalainen *et al*., 2008; Chandran, 2010; Kalin *et al*., 2010). IBDV, by interacting with the $\alpha 4\beta 1$-integrin (Delgui *et al*., 2009), can be considered as a new member of this group.

Birnaviruses form a unique family of naked dsRNA viruses infecting vertebrates and invertebrates (Delmas *et al*., 2005). This family groups viruses infecting both aquatic and terrestrial species, with *infectious necrosis pancreatic virus* (IPNV) and IBDV as prototype and best known species respectively (Da Costa *et al*., 2003). To date, there is scarce knowledge available regarding cellular internalization and intracellular trafficking of these viruses. Based on X-ray crystallographic structure of IPNV and IBDV subviral particles, it is evident that both viral agents share a highly similar capsid shell structure revealing the presence of a functional $\alpha 4\beta 1$ ligand motif identified as essential for IBDV cell attachment and infection (Delgui *et al*., 2009). Garriga *et al*. (2006) observed that, in a low Ca^{2+} ion concentration environment such as the endosome's (Gerasimenko *et al*., 1998), the trimeric structure of the IBDV VP2 protein in the viral capsid destabilizes facilitating the exposure of pep 46, the capsid-associated peptide was able to deform biological membranes leading to the formation of pores (Galloux *et al*., 2007). These observations comprised strong evidence towards the role of endocytosis in IBDV internalization. More recently, Yip *et al*. (2012) showed that a caIBDV was internalized in avian cells (DF-1 cells) mainly by caveolae/lipid raft mediated endocytosis. Because of a weak inhibition caused by the macropinocytosis inhibitors used, the authors proposed that caIBDV does not use macropinocytosis as the major endocytic route playing an assistant role for the endosomal escape during caIBDV entry. An important point to take into account regarding their findings is that the authors employed only an avian cell line in their study, and as they mentioned, concerns about the specificity of the inhibitors in DF-1 cells emerged. The present study constitutes the first systematic characterization of the endocytic pathway mediating the IBDV cell entry providing solid evidence that IBDV mainly exploits macropinocytosis to access the host cell and further traffics to the early endosomes. Because of the the strong conservation of the IBDV and IPNV capsid structures mentioned earlier, it is tempting to hypothesize that *Aquabirnaviruses* and other viruses of the family may also use this pathway to initiate their replication cycle.

Experimental procedures

Cells and virus

The IBDV Soroa strain, a virulent serotype 1 virus, was propagated in QM7 avian myoblasts cells (ATCC, CRL-1962) as previously described (Lombardo *et al.*, 1999). Human epithelial HeLa and QM7 cells were grown at 37°C in an atmosphere of 95% air and 5% CO_2 in Dulbecco's modified Eagle's medium (DMEM, Life Technologies, Buenos Aires, Argentina) containing 10% FCS (PAA Laboratories, Ciudad Autónoma de Buenos Aires, Argentina).

Antibodies and reagents

Western blot and confocal laser scanning microscopy (CLSM) analyses were carried out using the following primary antibodies: rabbit anti-VP3-specific sera as previously described (Fernandez-Arias *et al.*, 1998), rabbit anti-NHE-1 (Merck Millipore, Biopore, Argentine), kindly provided by Dr Victoria Bocanegra from IMBECU-CONICET, Mendoza, Argentina, monoclonal mouse anti-β tubulin from the Developmental Studies Hybridoma Bank (Iowa, USA) and mouse anti-actin from Sigma-Aldrich (Buenos Aires, Argentina). The secondary goat anti-rabbit antibodies conjugated with Alexa 488 or Cy3, and Hoechst 33342 were purchased from Molecular Probes (Life Technologies). Peroxidase-conjugated secondary antibodies were purchased from Sigma-Aldrich. Pharmacological inhibitors and control reagents were employed following the manufacturer's recommendations and at the indicated concentrations. Dyn (80 μM), CPZ (50 μM), MβCD (5 mM), Fil III (5 μg ml^{-1}), kindly provided by Dr Miguel Fornés (IHEM, U.N. Cuyo, CONICET), Cyto D (5 μM), Lat B (1.5 μM), Baf A1 (100 nM), and Lys (25 nM) were purchased from Sigma-Aldrich. EIPA (80 μM) was purchased from Life Technologies and ammonium chloride (NH_4Cl: 50 mM) was purchased from Química Dalton (Córdoba, Argentina). Wort (100 nM) and Y-27632 (10 μM) were purchased from Sigma-Aldrich. Trf-Alexa 633 and Trf-tetramethyl rhodamin conjugates (Trf: 5 μg ml^{-1}), Dx-Texas red conjugate 70 kD (Dx: 1 mg ml^{-1}) and CtB-Alexa 594 conjugate (10 μg ml^{-1}) were purchased from Molecular Probes (Life Technologies). Rhodamine-conjugated phalloidin was purchased from Sigma-Aldrich.

Plasmids and transfections

Plasmids encoding EGFP-Rab5wt and EGFP-Rab5Q67L were kindly provided by Dr Philip D. Stahl (Washington University, St Louis, MO, USA). The plasmid encoding EGFP-Rab5S34N was a generous gift from Dr Marino Zerial (Max Planck Institute of Molecular Cell Biology and Genetics, Dresden, Germany). Plasmids encoding EGFP-Rab7wt and EGFP-Rab7T22N were kindly provided by Dr Bo van Deurs (University of Copenhagen, Copenhagen, Denmark) and plasmids encoding EGFP-Dyn2wt and EGFP-Dyn2K44A were kindly provided by Dr Bruno Hernáez (CBM-CSIC, Madrid, Spain) and plasmids encoding EGFP-RhoA N19, EGFP-Rac1 N17 and EGFPCdc42 N17 were kindly provided by Dr Walter Berón (Institute of Histology and Embriology, Mendoza, Argentina). Plasmids were transfected in 80% confluent cells monolayers grown on coverslips using 2 μg of DNA and Lipofectamine Plus (Invitrogen, Life Technologies) following the manufacturer's recommendation. After 12 h, cells were infected with IBDV at a MOI of 1 pfu $cell^{-1}$ for 1 h. Cells were washed twice with phosphate-buffered saline (PBS) and the infection was allowed to proceed for an additional 12 or 24 h period. Finally, cells were fixed and prepared for immunofluorescence as described later.

Trf, Dx and CtB uptake assays

HeLa or QM7 cells grown in coverslips were left untreated or pretreated with the corresponding inhibitors (see later) and then incubated with 5 μg ml^{-1} Trf-tetramethyl rhodamine conjugate or Trf-Alexa 633 conjugate for 15 min, 10 μg ml^{-1} CtB-Alexa 594 conjugate for 30 min, 1 mg ml^{-1} Dx-Texas Red 70 kD for 60 min or 25 nM Lysotraker for 15 min at 37°C and then washed three times with PBS followed by additional three acid washes of 5 min (1.5 M citric acid PBS pH 5.5) to remove the unbound reagent. Finally, monolayers were mounted in Mowiol and analysed by CLSM.

Treatment of HeLa or QM7 cells with inhibitors

Confluent monolayers of HeLa or QM7 cells grown in six-wells plates were washed twice with PBS and were pretreated with the appropriate concentration of Dyn, CPZ, MβCD, Fil III, Cyto D, Lat B, EIPA, Wort; Y-27632, Baf A1 or NH_4Cl for 60 min. After the incubation period, cells were infected with IBDV at a MOI of 1 pfu $cell^{-1}$ for 1 h in the presence of the corresponding inhibitor. Cells were washed twice with PBS and the infection was left to proceed for additional 12 or 24 h in the case of MβCD or Fil III. The inhibitors were present during the entire infection/incubation period, except for the MβCD, which was present for the first 3 h of infection because of toxicity. After incubations, cells were processed for immunofluorescence analysis and Western blot analysis.

Test of lysosomal function by degradation of a chromogenic BSA

The ability of cells to endocytose and degrade the DQ-BSA, was used to measure EGFP-Rab7T22N interfering activity. Red DQ-BSA requires enzymatic cleavage in an acidic intracellular compartment (i.e. lysosomes) to generate a highly fluorescent product, which can be monitored by confocal microscopy. EGFP-Rab7T22N-transfected cells were incubated for 12 h at 37°C with DQ-BSA (10 μg ml^{-1} in complete culture medium) to assure that the reagent reaches the lysosomal compartment. Cells were washed and left an additional overnight period with fresh medium in the absence of the probe. Cells were fixed and analysed by CLSM.

Sodium dodecyl sulfate polyacrylamide gel electrophoresis (SDS-PAGE) and Western blot

Protein samples of a total cell lysate from mock or infected HeLa and QM7 cells were run on a 12% polyacrylamide gel and transferred to Hybond-ECL (GE Healthcare, Ciudad Autónoma de Buenos Aires, Argentina) nitrocellulose membranes. The membranes were blocked for 1 h with blocking solution (5% non-fat milk, 0.1% Tween 20 and PBS), washed twice with PBS and

incubated with a primary antibody anti-VP3, anti-β-tubulin or anti-β-actin and the corresponding peroxidase-conjugated secondary antibodies. Membranes were extensively washed, the corresponding bands were detected using an enhanced chemiluminescence detection kit from GE Healthcare, and data collected with an LAS-4000 imaging system (Fujifilm, Japan). The intensity of protein bands from three independent experiments were quantitated with the Adobe Photoshop CS5 software, and normalized against tubulin or actin. A paired Student's *t*-test was performed using the Ky-Plot software (version 2.0 beta 15). Representative images are shown for each case.

Indirect immunofluorescence

Immunofluorescence procedures were carried out at room temperature. Cells were fixed with a 3% paraformaldehyde solution in PBS for 15 min and quenched by incubating with 50 mM NH_4Cl in PBS for 20 min. Subsequently, cells were permeabilized with 0.05% saponin in PBS containing 0.2% BSA, incubated with primary antibodies and the corresponding Alexa 488- or Cy3-conjugated secondary antibodies. Cells were mounted with Mowiol (plus Hoechst stain) and analysed by CLSM. Images were captured using an Olympus FluoView TM FV1000 confocal microscope (Olympus, Ciudad Autónoma de Buenos Aires, Argentina), with the FV10-ASW (version 01.07.00.16) software and processed by using Adobe CS5 (Adobe Systems, California, United States). For quantification purposes, the percentage of infected cells was determined in control or treated cells. Data were acquired from at least three independent experiments and statistical analysis Student's *t*-test was performed using the Ky-Plot software. Representative images are shown for each case.

Fluid phase uptake

Subconfluent QM7 cells seeded over coverslips in 24 well plates were starved for a 4 h period of with serum-free DMEM medium. Afterwards, cells were either maintained with serum-free DMEM medium (control situation), incubated with DMEM containing 10% FCS to induce macropinocytosis or infected with IBDV or IBDV + EIPA at a MOI of 10 pfu $cell^{-1}$ for 60 min in the presence of 1 mg ml^{-1} 70 kD Dx-Texas Red. The cells were washed three times with PBS followed by an additional three acid washes of 5 min (1.5 M citric acid PBS pH 5.5), fixed in 3% formaldehyde and analysed by LSCM as described. For quantification, all the obtained images were processed using ImageJ software (Wayne Rasband, National Institutes of Health, Maryland, United States). Briefly, after background elimination, the Dx-Texas red dots number was determined using the particle analyser plug-in. For colocalization analysis, cells were fixed in 3% formaldehyde and processed as mentioned earlier. To detect the virus, specific antibodies anti-VP2 were employed, followed by the corresponding Cy3-secondary antibodies. Cells were mounted with Mowiol (plus Hoechst stain) and analysed by CLSM. Images were captured using an Olympus FluoView TM FV1000 confocal microscope (Olympus), with the FV10-ASW (version 01.07.00.16) software and processed using Adobe CS5 (Adobe Systems).

Actin rearrangements analysis

HeLa cells were incubated in DMEM as a control condition, or infected with IBDV at a MOI 10 pfu $cell^{-1}$ for 45 min prior to fixation with 3% paraformaldehyde and then processed for indirect immunofluorescence using anti-VP2 and the corresponding Alexa 488-conjugated secondary antibodies. Afterwards, monolayers were incubated with Phalloidin–Rhodamine (1:200) for 1 h at 37°C. Nuclei were stained with Hoechst (blue) and the coverslips were analysed by CLSM. The percentage of cells with normal or disorganized actin filaments in both conditions was determined.

Transmission electron microscopy

For morphological analysis and internalization kinetics, HeLa cells grown in p100 plates at 80% confluence were infected with IBDV at a MOI of 50 pfu/cell for 15, 45 and 60 min prior to fixation. In a different set of experiments cells untreated or pretreated for 60 min with 5 μM Cyto D or 1.5 μM Lat B were infected with IBDV at a MOI of 50 pfu $cell^{-1}$ and incubated in the presence of the drugs for an additional 60 min. Cells were fixed with 4% paraformaldehyde and 0.1% glutaraldehyde in PBS at 4°C for 30 min. Then, the samples were cryofixed by rapid immersion in liquid ethane employing a Leica EM-CPC equipment. After fixation, samples were cryo-substituted in methanol with 0.5% uranil acetate at −90°C for 50 min and embedded in Lowylcryl HM20 at −40°C and polymerized under ultraviolet light at −40°C for 48 h followed by 24 h at room temperature. Cryo-substitution was carried out employing a Leica EM AFS2 equipment (Leica Microsystems, Wetzlar, Germany). Ultrathin sections were prepared with a Leica Ultracut R (Leica Microsystems, Wetzlar, Germany). Sections of 60–100 nm were contrasted and viewed under a Zeiss 900 electron microscope (Oberkochen, Germany).

Acknowledgements

We thank Alejandra Medero, Rodrigo Militello, Marcelo Furlán and Graciela Gutierrez for valuable technical assistance. We are grateful to Cristina Patiño Martín and Javier Bueno Chamorro from the electron microscopy service from the CNB-CSIC, Madrid, Spain who helped us with sample preparation. We thank Sergio Milone and Stella Galfré, from Universidad Juan A. Maza, for valuable laboratory help. We also thank Elisa Bocanegra, Norberto Domizio and Jorge Ibañez for valuable technique assistance in electron microscopy handling, and Romy Dalton and Idoia Busnadiego for sharing their stocks of purified IBDV. We also thank Drs Walter Berón and Patricia Romano from the Instituto de Histología y Embriología de Mendoza, Mendoza, Argentina for sharing valuable reagents. This work was partly supported by grants from the Agencia Nacional de Promoción Científica y Tecnológica (PICT2008-0192; PICT2011-0455), and SeCTyP (Universidad Nacional de Cuyo) to M. I. C.; PIP-CONICET (#11420110100237), SeCTyP-UNCuyo (Code 06/M040) and U.Maza (Resolution 889/12, 7-11-2011) to L. R. D.; and AGL2011-24758 from the Spanish Ministry of Economy and Competitiveness to J. F. R.

References

Amstutz, B., Gastaldelli, M., Kalin, S., Imelli, N., Boucke, K., Wandeler, E., *et al.* (2008) Subversion of CtBP1-controlled macropinocytosis by human adenovirus serotype 3. *EMBO J* **27:** 956–969.

Araki, N., Egami, Y., Watanabe, Y., and Hatae, T. (2007) Phosphoinositide metabolism during membrane ruffling and macropinosome formation in EGF-stimulated A431 cells. *Exp Cell Res* **313:** 1496–1507.

van den Berg, T.P., Eterradossi, N., Toquin, D., and Meulemans, G. (2000) Infectious bursal disease (Gumboro disease). *Rev Sci Tech* **19:** 509–543.

Bottcher, B., Kiselev, N.A., Stel'Mashchuk, V.Y., Perevozchikova, N.A., Borisov, A.V., and Crowther, R.A. (1997) Three-dimensional structure of infectious bursal disease virus determined by electron cryomicroscopy. *J Virol* **71:** 325–330.

Bucci, C., Parton, R.G., Mather, I.H., Stunnenberg, H., Simons, K., Hoflack, B., and Zerial, M. (1992) The small GTPase rab5 functions as a regulatory factor in the early endocytic pathway. *Cell* **70:** 715–728.

Chandran, B. (2010) Early events in Kaposi's sarcoma-associated herpesvirus infection of target cells. *J Virol* **84:** 2188–2199.

Conner, S.D., and Schmid, S.L. (2003) Regulated portals of entry into the cell. *Nature* **422:** 37–44.

Cook, T.A., Urrutia, R., and McNiven, M.A. (1994) Identification of dynamin 2, an isoform ubiquitously expressed in rat tissues. *Proc Natl Acad Sci USA* **91:** 644–648.

Da Costa, B., Soignier, S., Chevalier, C., Henry, C., Thory, C., Huet, J.C., and Delmas, B. (2003) Blotched snakehead virus is a new aquatic birnavirus that is slightly more related to avibirnavirus than to aquabirnavirus. *J Virol* **77:** 719–725.

Delgui, L., Oña, A., Gutierrez, S., Luque, D., Navarro, A., Castón, J.R., and Rodríguez, J.F. (2009) The capsid protein of infectious bursal disease virus contains a functional alpha 4 beta 1 integrin ligand motif. *Virology* **386:** 360–372.

Delgui, L.R., Rodriguez, J.F., and Colombo, M.I. (2013) The endosomal pathway and the Golgi complex are involved in the Infectious Bursal Disease Virus life cycle. *J Virol* **87:** 8993–9007.

Delmas, B., Kibenge, F., Leong, J., Mundt, E., Vakharia, V., and Wu, J. (2005) *Birnaviridae. Virus Taxonomy*. London: Academic Press, pp. 561–569.

Doherty, G.J., and McMahon, H.T. (2009) Mechanisms of endocytosis. *Annu Rev Biochem* **78:** 857–902.

Feng, Y., Press, B., and Wandinger-Ness, A. (1995) Rab 7: an important regulator of late endocytic membrane traffic. *J Cell Biol* **131:** 1435–1452.

Ferguson, S.M., Brasnjo, G., Hayashi, M., Wolfel, M., Collesi, C., Giovedi, S., *et al*. (2007) A selective activity-dependent requirement for dynamin 1 in synaptic vesicle endocytosis. *Science* **316:** 570–574.

Fernandez-Arias, A., Risco, C., Martinez, S., Albar, J.P., and Rodriguez, J.F. (1998) Expression of ORF A1 of infectious bursal disease virus results in the formation of virus-like particles. *J Gen Virol* **79:** 1047–1054.

Galloux, M., Libersou, S., Morellet, N., Bouaziz, S., Da Costa, B., Ouldali, M., *et al*. (2007) Infectious bursal disease virus, a non-enveloped virus, possesses a capsid-associated peptide that deforms and perforates biological membranes. *J Biol Chem* **282:** 20774–20784.

Garriga, D., Querol-Audi, J., Abaitua, F., Saugar, I., Pous, J., Verdaguer, N., *et al*. (2006) The 2.6-Angstrom structure of infectious bursal disease virus-derived T = 1 particles reveals new stabilizing elements of the virus capsid. *J Virol* **80:** 6895–6905.

Gastaldelli, M., Imelli, N., Boucke, K., Amstutz, B., Meier, O., and Greber, U.F. (2008) Infectious adenovirus type 2 transport through early but not late endosomes. *Traffic* **9:** 2265–2278.

Gerasimenko, J.V., Tepikin, A.V., Petersen, O.H., and Gerasimenko, O.V. (1998) Calcium uptake via endocytosis with rapid release from acidifying endosomes. *Curr Biol* **8:** 1335–1338.

Gorvel, J.P., Chavrier, P., Zerial, M., and Gruenberg, J. (1991) rab5 controls early endosome fusion in vitro. *Cell* **64:** 915–925.

Hall, A. (1998) Rho GTPases and the actin cytoskeleton. *Science* **279:** 509–514.

Hall, A., and Nobes, C.D. (2000) Rho GTPases: molecular switches that control the organization and dynamics of the actin cytoskeleton. *Philos Trans R Soc Lond B Biol Sci* **355:** 965–970.

Hernaez, B., and Alonso, C. (2010) Dynamin- and clathrin-dependent endocytosis in African swine fever virus entry. *J Virol* **84:** 2100–2109.

Kaksonen, M., Toret, C.P., and Drubin, D.G. (2006) Harnessing actin dynamics for clathrin-mediated endocytosis. *Nat Rev Mol Cell Biol* **7:** 404–414.

Kalin, S., Amstutz, B., Gastaldelli, M., Wolfrum, N., Boucke, K., Havenga, M., *et al*. (2010) Macropinocytotic uptake and infection of human epithelial cells with species B2 adenovirus type 35. *J Virol* **84:** 5336–5350.

Kanzaki, M., and Pessin, J.E. (2002) Caveolin-associated filamentous actin (Cav-actin) defines a novel F-actin structure in adipocytes. *J Biol Chem* **277:** 25867–25869.

Karjalainen, M., Kakkonen, E., Upla, P., Paloranta, H., Kankaanpaa, P., Liberali, P., *et al*. (2008) A Raft-derived, Pak1-regulated entry participates in alpha2beta1 integrin-dependent sorting to caveosomes. *Mol Biol Cell* **19:** 2857–2869.

Karmazyn, M. (2013) NHE-1: still a viable therapeutic target. *J Mol Cell Cardiol* **61:** 77–82.

Keen, J.H. (1990) Clathrin and associated assembly and disassembly proteins. *Annu Rev Biochem* **59:** 415–438.

Kerr, M.C., and Teasdale, R.D. (2009) Defining macropinocytosis. *Traffic* **10:** 364–371.

Kilsdonk, E.P., Yancey, P.G., Stoudt, G.W., Bangerter, F.W., Johnson, W.J., Phillips, M.C., and Rothblat, G.H. (1995) Cellular cholesterol efflux mediated by cyclodextrins. *J Biol Chem* **270:** 17250–17256.

Koivusalo, M., Welch, C., Hayashi, H., Scott, C.C., Kim, M., Alexander, T., *et al*. (2010) Amiloride inhibits macropinocytosis by lowering submembranous pH and preventing Rac1 and Cdc42 signaling. *J Cell Biol* **188:** 547–563.

Kojima, A., Toshima, J.Y., Kanno, C., Kawata, C., and Toshima, J. (2012) Localization and functional requirement of yeast Na+/H+ exchanger, Nhx1p, in the endocytic and protein recycling pathway. *Biochim Biophys Acta* **1823:** 534–543.

Kranenburg, O., Verlaan, I., and Moolenaar, W.H. (2001) Regulating c-Ras function. cholesterol depletion affects

caveolin association, GTP loading, and signaling. *Curr Biol* **11:** 1880–1884.

Krzyzaniak, M.A., Zumstein, M.T., Gerez, J.A., Picotti, P., and Helenius, A. (2013) Host cell entry of respiratory syncytial virus involves macropinocytosis followed by proteolytic activation of the F protein. *PLoS Pathog* **9:** e1003309.

Li, G., and Stahl, P.D. (1993) Structure-function relationship of the small GTPase rab5. *J Biol Chem* **268:** 24475–24480.

Liberali, P., Ramo, P., and Pelkmans, L. (2008) Protein kinases: starting a molecular systems view of endocytosis. *Annu Rev Cell Dev Biol* **24:** 501–523.

Liebl, D., and Griffiths, G. (2009) Transient assembly of F-actin by phagosomes delays phagosome fusion with lysosomes in cargo-overloaded macrophages. *J Cell Sci* **122:** 2935–2945.

Lin, T.W., Lo, C.W., Lai, S.Y., Fan, R.J., Lo, C.J., Chou, Y.M., *et al*. (2007) Chicken heat shock protein 90 is a component of the putative cellular receptor complex of infectious bursal disease virus. *J Virol* **81:** 8730–8741.

Lindmo, K., and Stenmark, H. (2006) Regulation of membrane traffic by phosphoinositide 3-kinases. *J Cell Sci* **119:** 605–614.

Lombardo, E., Maraver, A., Caston, J.R., Rivera, J., Fernandez-Arias, A., Serrano, A., *et al*. (1999) VP1, the putative RNA-dependent RNA polymerase of infectious bursal disease virus, forms complexes with the capsid protein VP3, leading to efficient encapsidation into virus-like particles. *J Virol* **73:** 6973–6983.

Lu, L., Khan, S., Lencer, W., and Walker, W.A. (2005) Endocytosis of cholera toxin by human enterocytes is developmentally regulated. *Am J Physiol Gastrointest Liver Physiol* **289:** G332–G341.

Luque, D., Saugar, I., Rejas, M.T., Carrascosa, J.L., Rodriguez, J.F., and Caston, J.R. (2009) Infectious bursal disease virus: ribonucleoprotein complexes of a double-stranded RNA virus. *J Mol Biol* **386:** 891–901.

Macia, E., Ehrlich, M., Massol, R., Boucrot, E., Brunner, C., and Kirchhausen, T. (2006) Dynasore, a cell-permeable inhibitor of dynamin. *Dev Cell* **10:** 839–850.

Marechal, V., Prevost, M.C., Petit, C., Perret, E., Heard, J.M., and Schwartz, O. (2001) Human immunodeficiency virus type 1 entry into macrophages mediated by macropinocytosis. *J Virol* **75:** 11166–11177.

Marshansky, V., and Futai, M. (2008) The V-type H+-ATPase in vesicular trafficking: targeting, regulation and function. *Curr Opin Cell Biol* **20:** 415–426.

Masereel, B., Pochet, L., and Laeckmann, D. (2003) An overview of inhibitors of Na(+)/H(+) exchanger. *Eur J Med Chem* **38:** 547–554.

Meier, O., Boucke, K., Hammer, S.V., Keller, S., Stidwill, R.P., Hemmi, S., and Greber, U.F. (2002) Adenovirus triggers macropinocytosis and endosomal leakage together with its clathrin-mediated uptake. *J Cell Biol* **158:** 1119–1131.

Menon, M., and Schafer, D.A. (2013) Dynamin: expanding its scope to the cytoskeleton. *Int Rev Cell Mol Biol* **302:** 187–219.

Mercer, J., and Greber, U.F. (2013) Virus interactions with endocytic pathways in macrophages and dendritic cells. *Trends Microbiol* **21:** 380–388.

Mercer, J., and Helenius, A. (2009) Virus entry by macropinocytosis. *Nat Cell Biol* **11:** 510–520.

Mercer, J., and Helenius, A. (2012) Gulping rather than sipping: macropinocytosis as a way of virus entry. *Curr Opin Microbiol* **15:** 490–499.

Mercer, J., Schelhaas, M., and Helenius, A. (2010) Virus entry by endocytosis. *Annu Rev Biochem* **79:** 803–833.

Merrifield, C.J. (2004) Seeing is believing: imaging actin dynamics at single sites of endocytosis. *Trends Cell Biol* **14:** 352–358.

Monis, G.F., Schultz, C., Ren, R., Eberhard, J., Costello, C., Connors, L., *et al*. (2006) Role of endocytic inhibitory drugs on internalization of amyloidogenic light chains by cardiac fibroblasts. *Am J Pathol* **169:** 1939–1952.

Morlot, S., and Roux, A. (2013) Mechanics of dynamin-mediated membrane fission. *Annu Rev Biophys* **42:** 629–649.

Mukhopadhyay, A., Barbieri, A.M., Funato, K., Roberts, R., and Stahl, P.D. (1997) Sequential actions of Rab5 and Rab7 regulate endocytosis in the *Xenopus oocyte*. *J Cell Biol* **136:** 1227–1237.

Nanbo, A., Imai, M., Watanabe, S., Noda, T., Takahashi, K., Neumann, G., *et al*. (2010) Ebola virus is internalized into host cells via macropinocytosis in a viral glycoprotein-dependent manner. *PLoS Pathog* **6:** e1001121.

Niedergang, F., and Chavrier, P. (2005) Regulation of phagocytosis by Rho GTPases. *Curr Top Microbiol Immunol* **291:** 43–60.

Nobes, C.D., and Hall, A. (1995) Rho, rac, and cdc42 GTPases regulate the assembly of multimolecular focal complexes associated with actin stress fibers, lamellipodia, and filopodia. *Cell* **81:** 53–62.

Norbury, C.C. (2006) Drinking a lot is good for dendritic cells. *Immunology* **117:** 443–451.

Ohkuma, S., and Poole, B. (1978) Fluorescence probe measurement of the intralysosomal pH in living cells and the perturbation of pH by various agents. *Proc Natl Acad Sci USA* **75:** 3327–3331.

Orlandi, P.A., and Fishman, P.H. (1998) Filipin-dependent inhibition of cholera toxin: evidence for toxin internalization and activation through caveolae-like domains. *J Cell Biol* **141:** 905–915.

Orlowski, J., and Grinstein, S. (2004) Diversity of the mammalian sodium/proton exchanger SLC9 gene family. *Pflugers Arch* **447:** 549–565.

Parton, R.G., and Richards, A.A. (2003) Lipid rafts and caveolae as portals for endocytosis: new insights and common mechanisms. *Traffic* **4:** 724–738.

Patel, J.C., and Galan, J.E. (2006) Differential activation and function of Rho GTPases during Salmonella–host cell interactions. *J Cell Biol* **175:** 453–463.

Pelkmans, L., Puntener, D., and Helenius, A. (2002) Local actin polymerization and dynamin recruitment in SV40-induced internalization of caveolae. *Science* **296:** 535–539.

Peterson, J.R., and Mitchison, T.J. (2002) Small molecules, big impact: a history of chemical inhibitors and the cytoskeleton. *Chem Biol* **9:** 1275–1285.

Pike, L.J., and Miller, J.M. (1998) Cholesterol depletion delocalizes phosphatidylinositol bisphosphate and inhibits hormone-stimulated phosphatidylinositol turnover. *J Biol Chem* **273:** 22298–22304.

Ridley, A.J. (2006) Rho GTPases and actin dynamics in membrane protrusions and vesicle trafficking. *Trends Cell Biol* **16:** 522–529.

Rink, J., Ghigo, E., Kalaidzidis, Y., and Zerial, M. (2005) Rab conversion as a mechanism of progression from early to late endosomes. *Cell* **122:** 735–749.

Rojas, A.M., Fuentes, G., Rausell, A., and Valencia, A. (2012) The Ras protein superfamily: evolutionary tree and role of conserved amino acids. *J Cell Biol* **196:** 189–201.

Rupper, A., Lee, K., Knecht, D., and Cardelli, J. (2001) Sequential activities of phosphoinositide 3-kinase, PKB/Aakt, and Rab7 during macropinosome formation in *Dictyostelium*. *Mol Biol Cell* **12:** 2813–2824.

Saeed, M.F., Kolokoltsov, A.A., Albrecht, T., and Davey, R.A. (2010) Cellular entry of ebola virus involves uptake by a macropinocytosis-like mechanism and subsequent trafficking through early and late endosomes. *PLoS Pathog* **6:** e1001110.

Schelhaas, M., Shah, B., Holzer, M., Blattmann, P., Kuhling, L., Day, P.M., *et al*. (2012) Entry of human papillomavirus type 16 by actin-dependent, clathrin- and lipid raft-independent endocytosis. *PLoS Pathog* **8:** e1002657.

Sharma, J.M., Kim, I.J., Rautenschlein, S., and Yeh, H.Y. (2000) Infectious bursal disease virus of chickens: pathogenesis and immunosuppression. *Dev Comp Immunol* **24:** 223–235.

Stenmark, H., Parton, R.G., Steele-Mortimer, O., Lutcke, A., Gruenberg, J., and Zerial, M. (1994) Inhibition of rab5 GTPase activity stimulates membrane fusion in endocytosis. *EMBO J* **13:** 1287–1296.

Swanson, J.A., and Watts, C. (1995) Macropinocytosis. *Trends Cell Biol* **5:** 424–428.

Valiya Veettil, M., Sadagopan, S., Kerur, N., Chakraborty, S., and Chandran, B. (2010) Interaction of c-Cbl with myosin IIA regulates Bleb associated macropinocytosis of Kaposi's sarcoma-associated herpesvirus. *PLoS Pathog* **6:** e1001238.

Vitelli, R., Santillo, M., Lattero, D., Chiariello, M., Bifulco, M., Bruni, C.B., and Bucci, C. (1997) Role of the small GTPase Rab7 in the late endocytic pathway. *J Biol Chem* **272:** 4391–4397.

de Vries, E., Tscherne, D.M., Wienholts, M.J., Cobos-Jimenez, V., Scholte, F., Garcia-Sastre, A., *et al*. (2011) Dissection of the influenza A virus endocytic routes reveals macropinocytosis as an alternative entry pathway. *PLoS Pathog* **7:** e1001329.

Wang, L.H., Rothberg, K.G., and Anderson, R.G. (1993) Mis-assembly of clathrin lattices on endosomes reveals a regulatory switch for coated pit formation. *J Cell Biol* **123:** 1107–1117.

West, M.A., Bretscher, M.S., and Watts, C. (1989) Distinct endocytotic pathways in epidermal growth factor-stimulated human carcinoma A431 cells. *J Cell Biol* **109:** 2731–2739.

Yamauchi, Y., and Helenius, A. (2013) Virus entry at a glance. *J Cell Sci* **126:** 1289–1295.

Yip, C.W., Hon, C.C., Zeng, F., and Leung, F.C. (2012) Cell culture-adapted IBDV uses endocytosis for entry in DF-1 chicken embryonic fibroblasts. *Virus Res* **165:** 9–16.

Zerial, M., and McBride, H. (2001) Rab proteins as membrane organizers. *Nat Rev Mol Cell Biol* **2:** 107–117.

Supporting information

Additional Supporting Information may be found in the online version of this article at the publisher's web-site:

Fig. S1. Treatment of QM7 cells with the pharmacological inhibitors. (A) Cells untreated or pretreated with Dyn or CPZ were incubated with Transferrin-Rhodamine. (B) Cells untreated or pretreated with Cyto D, Lat B or EIPA were incubated with Dx-Texas Red 70 kD. Subsequently, the cells in A and B, were extensively washed to remove the unbound tracer (in the case of Dextran, an acid wash was performed), and processed for CLSM. Mean fluorescence intensity of the fluorophore in each condition was calculated using ImageJ program employing 50 cells per condition. Scale bars represent 20 μm. (C) Mean fluorescence intensity corresponding to Transferrin-Alexa 633 internalization experiments shown in Fig. 1A.

Fig. S2. Control assays associated to trafficking experiments. (A) HeLa cells were untreated or pretreated with NH_4Cl or Baf A1 and incubated with Lysotracker-Red. Afterwards, cells were fixed and analysed as described. (B) HeLa or QM7 cells were transfected with GFP-tagged forms of the Dominant-negative mutants of Rab5 (EGFP-Rab5S34N) or Rab7 (EGFP-Rab7T22N) and incubated with Dx-Texas Red or DQ-BSA. At the indicated times, the monolayers were extensively washed to remove the unbound reagents (in the case of Dextran, an acid wash was performed) and processed for CSLM. Transfected cells are delineated showing the impaired traffic of the corresponding tracer. Scale bars represent 20 μm.